HHS Public Access

Author manuscript

Nat Microbiol. Author manuscript; available in PMC 2023 December 01.

Published in final edited form as:

Nat Microbiol. 2023 June ; 8(6): 1095–1107. doi:10.1038/s41564-023-01383-1.

Age-associated features of norovirus infection analyzed in mice

Elizabeth A. Kennedy[1], **Somya Aggarwal**[1], **Arko Dhar**[1], **Stephanie M. Karst**[2], **Craig B. Wilen**[3], **Megan T. Baldridge**[1,4,#]

[1]Division of Infectious Diseases, Department of Medicine, Edison Family Center for Genome Sciences & Systems Biology, Washington University School of Medicine, St. Louis, MO, USA

[2]Department of Molecular Genetics and Microbiology, College of Medicine, University of Florida, Gainesville, FL, USA.

[3]Departments of Laboratory Medicine & Immunobiology, Yale School of Medicine, New Haven, CT, USA

[4]Department of Molecular Microbiology, Washington University School of Medicine, St. Louis, MO, USA.

Abstract

Norovirus (NoV) is the leading global cause of viral gastroenteritis. Young children bear the highest burden of disease and play a key role in viral transmission throughout the population. However, which host factors contribute to age-associated variability in NoV severity and shedding are not well-defined. The murine NoV (MNoV) strain CR6 causes persistent infection in adult mice and targets intestinal tuft cells. Here, we find that natural transmission of CR6 from infected dams occurred only in juvenile mice. Direct oral CR6 inoculation of wild-type neonatal mice led to accumulation of viral RNA in the ileum that was replication-independent, induced both innate and adaptive immune responses including interferon-stimulated gene expression and MNoV-specific antibody responses, and was shed into stool for prolonged periods. Interestingly, viral uptake depended on passive ileal absorption of luminal virus, a process blocked by cortisone acetate administration which prevented ileal viral RNA accumulation. Neonates lacking interferon signaling in hematopoietic cells were susceptible to productive infection, viral dissemination and lethality, which depended on the canonical MNoV receptor CD300LF. Together, our findings reveal developmentally-associated aspects of persistent MNoV infection, including distinct tissue and cellular tropism, mechanisms of interferon regulation, and severity of infection in the absence of interferon signaling. These emphasize the importance of defining viral pathogenesis phenotypes across the developmental spectrum and highlight passive viral uptake as an important contributor to enteric infections in early life.

[#]Correspondence: mbaldridge@wustl.edu.

Author contributions: E.A.K, A.D., and S.A. performed the experiments. E.A.K. and M.T.B. analyzed the results. E.A.K., S.M.K., C.B.W. and M.T.B. designed the project. E.A.K. and M.T.B. wrote the manuscript. All authors read and edited the manuscript.

Competing interests: We declare no competing interests.

Reviewer Recognition:

Nature Microbiology thanks Nihal Altan-Bonnet, Jason Mackenzie and the other, anonymous, reviewer(s) for their contribution to the peer review of this work.

Editor summary:

Comparing norovirus infection in neonate and adult mice suggests age-dependent differences in passive viral uptake, cellular tropism, interferon regulation and viral dissemination.

Introduction

Norovirus (NoV) is the leading cause of acute gastroenteritis worldwide, affecting individuals of all ages but causing particularly high morbidity and mortality in children younger than five. Young children bear the highest burden of disease[1], with 66-90% experiencing at least one NoV infection before age three[2]. They often exhibit more prolonged and higher levels of fecal viral shedding than older children or adults[3,4], contributing to their central role in viral transmission to all age groups[5]. Although no vaccines or treatments for NoV currently exist, development of therapies targeting persistent NoV shedding in children could reduce fecal-oral spread throughout the entire population.

MNoV (MNoV) is a natural mouse pathogen that shares features of human NoVs including fecal-oral transmission, mechanisms of genome replication, and virion structure, serving as a powerful model for *in vivo* studies of pathogenesis[6]. Different MNoV strains model different aspects of human NoV infection. Acute strains infect gut-associated hematopoietic cells and are cleared by 7-14 days post-infection (dpi) in wild-type mice[7,8]. Conversely, persistent strains infect rare intestinal epithelial tuft cells and are shed in feces of wild-type animals through at least 70dpi[9,10], modeling human persistent asymptomatic shedding. All MNoV strains tested to date use the host protein CD300LF as a receptor[11-13]. Interferons (IFNs) are central for innate immune control of MNoV, with type III IFNs limiting intestinal viral replication and type I IFNs limiting viral dissemination to systemic tissues[14-17] and pathogenesis of acute strains[18]. Importantly, most studies characterizing MNoV pathogenesis have used adult mice, although NoV is an important cause of pediatric gastroenteritis.

It was recently reported that wild-type neonatal mice develop diarrhea after infection with an acute strain of MNoV, whereas persistent strains of MNoV cause substantially less diarrhea[19,20]. Whether persistent MNoV contributes to ongoing shedding in neonates remains unknown. To develop a model of persistent pediatric infection, we examined the dynamics and host factors involved in neonatal infection with persistent MNoV strain CR6. We found that transmission from infected dams to naïve pups occurs after postnatal day (P)16. However, after direct inoculation at P6, viral genomes are detected in stool until 10dpi. Intriguingly, in wild-type neonates, viral RNA is uniquely detected in ilea, and viral RNA presence is largely independent of tuft cells or CD300 viral receptors, both of which are required for CR6 infection of adults. Viral RNA ileal uptake and fecal shedding are unaffected by antiviral treatment but blocked by cortisone, which limits nonspecific uptake in the neonatal ileum. In contrast, when type I and II IFN signaling are disrupted, specifically in hematopoietic cells, CD300-dependent viral dissemination and lethality follow neonatal CR6 inoculation. Our data demonstrate passive ileal absorption as an understudied mechanism for enteric viral uptake in neonates, which is counterbalanced by host IFN signaling in hematopoietic cells to limit dissemination.

Results

Natural transmission of CR6 occurs after postnatal day 16

We initially investigated transmission of MNoV strain CR6 from infected dams to their naïve litters before weaning at postnatal day (P)21. Most pups did not shed viral RNA early in life, but almost all began shedding in the transition from P16 to P21 (Fig. 1A, 1B). CR6 was not detectable in ilea or colons of pups at P6 or P13, but was present at P21 (Fig. 1C, D). Transmission between P16 and P21 is consistent with the age at which pups become coprophagic[21] and could be naturally infected from the dam's stool.

CR6 inoculation associated with age-dependent tissue tropism

To directly assess early-life infection, we orally inoculated mice with CR6 at P6 (neonates), P15 (juveniles), or between 6-9 weeks of age (adults). All inoculated mice shed viral RNA in their feces between 3-10dpi, with neonates shedding significantly more than juveniles or adults at early time points (Fig. 2A-C). At 7dpi, ileal viral RNA was comparable between mice inoculated at different ages, although trended lower in juvenile mice (p=0.1187 versus adults, p=0.0842 versus neonates) (Fig. 2D). Viral RNA was nearly undetectable in neonatal colons, in contrast to substantial colonic viral RNA in juveniles and adults, suggesting age-dependent differences in CR6 localization (Fig. 2E).

Intestinal microbiota composition varies between mice from different vendors[22] or different genetic backgrounds[23]. Because commensal bacteria promote persistent MNoV infection of adult mice[24], we compared CR6 fecal shedding from C57BL/6 neonates sourced from Charles River (CR), Jackson Laboratories (JAX), or bred at Washington University in St. Louis (WUSTL). JAX neonates shed more viral RNA than WUSTL or CR neonates (Extended Data Fig. 1A). Among a variety of genetic backgrounds sourced from JAX, C57BL/6 shed at the highest levels (Extended Data Fig. 1B). BALB/c are more susceptible to rotavirus than C57BL/6 neonates[25], and both are susceptible to diarrhea after infection with acute MNoV strains[19,20]. While ileal and stool CR6 RNA were comparable between BALB/c and C57BL/6 pups at 7dpi, BALB/c pups exhibited higher colonic viral RNA (Extended Data Fig. 1C, D). Interestingly, adult BALB/c mice exhibited decreased stool viral RNA and trended towards decreased intestinal viral RNA (Extended Data Fig. 1E, F). Genetic background and microbiota may thus differentially influence CR6 localization throughout life.

Tuft cells are dispensable for neonatal CR6 RNA shedding

Intestinal tuft cells are the target of persistent CR6 infection in adult mice[10]. We inoculated neonatal and juvenile *Pou2f3*$^{-/-}$ mice, which lack tuft cells[26], and found that fecal shedding of CR6 RNA was independent of tuft cells in neonates (Fig. 3A), but dependent on tuft cells in juveniles (Fig. 3B). Dynamics of tuft cell development remain unclear, as some studies suggest that tuft cells develop prenatally[27] while others report that they do not accumulate until weaning[28]. In our mice, tuft cells, quantified by staining for marker DCLK1, were rare at P6 and P13 (Fig. 3C and Extended Data Fig. 2A). By P21, tuft cells remained rare in ileum but reached adult-like levels in colon. Co-staining for MNoV nonstructural protein NS6/7 showed no CR6-positive tuft cells at 7dpi in neonates, compared to detectable

co-localization in adults (Fig. 3D). We similarly failed to observe non-tuft NS6/7-positive cells in the neonatal ileum. Altogether, our findings suggest that intestinal tuft cells are rare during early life and neonatal CR6 RNA shedding is independent of tuft cells.

CD300LF is largely dispensable for neonatal CR6 RNA shedding

In adult mice, CD300LF expression on tuft cells is required for CR6 infection[8,12,13]. Among intestinal epithelial cells (IECs), CD300LF is expressed exclusively on tuft cells[10,29], but cells including macrophages and dendritic cells express CD300LF and are permissive to other MNoV strains[8]. *Cd300lf* expression in the colon was low early in life, but reached adult-like levels by P21, mirroring colonic tuft cell development (Extended Data Fig. 2B). In contrast, ileal *Cd300lf* expression was age-independent, suggesting that non-tuft cells expressing CD300LF could support CR6 RNA shedding. *Cd300lf*$^{-/-}$ mice shed viral RNA after neonatal but not juvenile inoculation (Fig. 3A, 3B), although *Cd300lf*$^{-/-}$ neonates shed less viral RNA than wild-type neonates (Fig. 3A) and exhibited decreased viral RNA in MLNs and spleen but not ilea (Fig. 3E), suggesting a partial role for CD300LF in neonatal viral RNA uptake. To confirm this, we pre-incubated CR6 with Fc-fusion proteins with either the mouse CD300LF ectodomain (Fc-msCD300LF), which neutralizes MNoV[30], or a human CD300LF ectodomain control (Fc-huCD300LF)[13]. Fc-msCD300LF, but not Fc-huCD300LF, blocked CR6 infection of BV2 microglia cells *in vitro* (Extended Data Fig. 3). Neonates inoculated with CR6 pre-incubated with Fc-msCD300LF exhibited reduced CR6 RNA shedding (Fig. 3F) and intestinal viral RNA (Fig. 3G), although substantial viral RNA remained detectable in stool and ilea. These data support that CD300LF is partially involved in, but not necessary for, neonatal CR6 RNA uptake and shedding.

We hypothesized that another CD300 family member, CD300LD, may be involved in neonatal viral RNA shedding as CD300LD expression permits MNoV infection *in vitro*[11,12]. We found that *Cd300lf*$^{-/-}$*Cd300ld*$^{-/-}$ neonates shed comparable viral RNA to *Cd300lf*$^{-/-}$ neonates (Fig. 3A), whereas juvenile mice shed no virus (Fig. 3B). Thus, CD300LD is not responsible for CD300LF-independent early life viral RNA release.

STAT1 controls CR6 lethality and dissemination in neonates

In adult mice, CR6 replication is controlled by innate immune responses, particularly IFN pathways[15]. In contrast, neonatal *Rag1*$^{-/-}$ mice lacking B and T cells have higher viral titers after infection with acute MNoV strains, indicating adaptive immune control[19]. Neonatal CR6 inoculation induced IFN-stimulated genes (ISGs) *Ifit1* and *Mx2* in the ileum at 1 and 7dpi (Fig. 4A, B; Extended Data Fig. 4A, B), an induction not observed in colon (Extended Data Fig. 4C). Additionally, CR6-inoculated neonates generated serum anti-MNoV IgM and IgG responses at 14dpi (Fig. 4C, D), demonstrating that both innate and adaptive immune systems respond to neonatal inoculation. To test the contribution of innate and adaptive immunity in CR6 control, we infected *Stat1*$^{-/-}$, which lack a key transcription factor in IFN signaling, and *Rag1*$^{-/-}$ neonates. Fecal shedding in both was equivalent to wild-type neonates at 7dpi (Fig. 4E). Unexpectedly, *Stat1*$^{-/-}$ neonates succumbed to infection with CR6, exhibiting ~75% lethality by 14dpi (Fig. 4F). This contrasts with adult *Stat1*$^{-/-}$ mice, which rarely die after CR6 infection[31,32]. No lethality was observed in *Rag1*$^{-/-}$ neonates,

suggesting that regulation of viral pathogenesis is specific to IFN responses rather than altered priming of adaptive responses.

We next asked which type(s) of IFNs limit CR6-associated neonatal lethality. Neonates lacking *Ifnar1*, *Ifngr1*, or *Ifnlr1*, necessary for type I, II, and III IFN signaling respectively, did not succumb to infection (Fig. 4G). In adult mice, type I and II IFNs combinatorially limit lethality after acute MNoV infection[33], and indeed *Ifnar1*$^{-/-}$*Ifngr1*$^{-/-}$ neonates succumbed to CR6 infection (Fig. 4G). We also sought to define the cell type(s) in which *Stat1* expression prevents CR6 lethality. *Villin-Cre+;Stat1*$^{f/f}$ and *Lysm-Cre+;Stat1*$^{f/f}$ neonates, which lack *Stat1* expression in epithelial and myeloid cells respectively, survived infection (Fig. 4H). In contrast, *Vav-iCre+;Stat1*$^{f/f}$ neonates, lacking *Stat1* in hematopoietic and tuft cells, exhibited increased lethality versus littermate controls (Fig. 4H). Adult *Stat1*$^{-/-}$ mice exhibit increased intestinal and extraintestinal virus after CR6 infection[32]. Similarly, intestinal virus levels were higher in *Stat1*$^{-/-}$ versus wild-type neonates, and virus disseminated to extraintestinal sites in *Stat1*$^{-/-}$ neonates (Fig. 4I). Intestinal and systemic viral RNA was also higher in *Vav-iCre+;Stat1*$^{f/f}$ neonates compared to littermates (Fig. 4J). Additionally, we detected enhanced CR6 RNA in *Stat1*$^{-/-}$ ilea using RNA *in situ* hybridization (RNA-ISH) (Fig. 4K). Together, these data suggest that type I and II IFN signaling, acting at least partly in hematopoietic cells, limit viral replication, dissemination, and lethality after neonatal CR6 inoculation.

We also assessed whether CR6 pathogenesis in *Stat1*$^{-/-}$ mice was CD300-dependent. *Stat1*$^{-/-}$*CD300lf*$^{-/-}$ and *Stat1*$^{-/-}$*CD300lf*$^{-/-}$*Cd300ld*$^{-/-}$ neonates inoculated with CR6 exhibited significantly reduced lethality compared to *Stat1*$^{-/-}$ neonates (Fig. 4L), with reduced intestinal viral RNA and no detectable dissemination to spleen or brain (Fig. 4M). CR6 dissemination and pathogenesis in *Stat1*$^{-/-}$ neonates is thus CD300 receptor-dependent. Intriguingly, substantial viral RNA was still present in *Stat1*$^{-/-}$*CD300lf*$^{-/-}$ and *Stat1*$^{-/-}$*CD300lf*$^{-/-}$*Cd300ld*$^{-/-}$ ilea (Fig. 4M), and fecal viral RNA was comparable to *Stat1*$^{-/-}$ mice (Fig. 4N), similar to observations in *Cd300lf*$^{-/-}$ and *Cd300lf*$^{-/-}$*Cd300ld*$^{-/-}$ neonates (Fig. 3A, E). We therefore sought to further characterize the ileal and stool CR6 RNA in neonatal mice.

CR6 replicates in *Stat1*$^{-/-}$ but minimally in wild-type neonates

To delineate the nature of CD300-independent CR6 RNA shedding in neonates, we treated mice with viral polymerase inhibitor 2'-C-methylcytidine (2-CMC), which limits CR6 replication and shedding in adult mice (Extended Data Fig. 5)[34]. 2-CMC treatment beginning at 3dpi protected *Stat1*$^{-/-}$ neonates from lethality (Fig. 5A). While we were unable to directly compare tissue viral levels within these experiments, as untreated mice succumbed to infection by 7dpi, we observed lower viral RNA in 2-CMC-treated *Stat1*$^{-/-}$ neonates across tissues compared to prior experiments (compared to Fig. 4I; average $10^{4.1}$ in untreated versus $10^{2.4}$ brain MNoV genome copies in 2-CMC-treated mice), suggesting that 2-CMC limits CR6 dissemination in *Stat1*$^{-/-}$ neonates (Fig. 5B). However, stool viral RNA in *Stat1*$^{-/-}$ neonates was unaffected by 2-CMC treatment (Fig. 5C). Similarly, 2-CMC treatment beginning at 3dpi did not reduce ileal or stool viral RNA in wild-type mice at 7dpi. When antiviral treatment began at 0dpi, ileal and stool viral RNA decreased subtly

but remained detectable (Fig. 5D, E). Thus, while CR6 may replicate immediately after inoculation in wild-type neonates, viral RNA in the ileum and stool at later time points is predominantly independent of viral replication.

We questioned whether the detected virus was infectious, as viral nucleic acids may be shed in the absence of infectious virus[35]. While tissues and stool from adult mice produced plaques on BV2 cells *in vitro*, no plaques were detected from samples of wild-type neonates at 3-10dpi (Fig. 5F, G). 1 and 2dpi neonatal stool produced plaques, consistent with passage of infectious inoculum (Extended Data Fig. 6A). Samples from *Stat1*$^{-/-}$ neonates produced plaques (Fig. 5H, I), suggesting that infectious virus is produced in neonates lacking IFN signaling. Additionally, dsRNA and MNoV nonstructural viral protein NS6/7 colocalized with CD45 in spleen from *Stat1*$^{-/-}$ neonates, supporting viral replication in hematopoietic cells (Fig. 5J, Extended Data Fig. 6B-D). Together, these data suggest that IFNs limit production of infectious CR6 in neonates, and CR6 RNA detected in ilea and stool of immunocompetent neonates is not due to replicative infection.

CR6 does not persistently infect mice inoculated as neonates

We next assessed how long viral RNA remained detectable in the stool of mice inoculated as neonates. At 14dpi, CR6 RNA presence in stool depended on the infection status of the litter's dam (Fig. 5K). As the dam was not directly inoculated, maternal infection likely occurred via coprophagy early after pup inoculation, and infected dams could transfer virus to pups after P16 as in Fig. 1. Without maternal infection, neonates generally shed no fecal viral RNA at 14dpi. Similarly, *Cd300lf*$^{-/-}$ neonates largely cleared fecal viral RNA by 14dpi (Fig. 5L). These data suggest that early-life CR6 inoculation does not lead to persistent infection without secondary transmission from infected dams.

Finally, to identify the source of viral RNA in wild-type neonatal stool, we assessed IEC extrusion, which is induced by rotavirus infection in neonatal mice[36]. We quantified expression of murine housekeeping gene *Rps29* in fecal samples of CR6-inoculated mice. CR6 inoculation increased IEC extrusion in adult but not neonatal mice (Fig. 5M). However, extrusion was markedly higher in P13 neonates than P20 or adult mice. CR6 RNA in neonatal stool may thus originate from extruded IECs.

CR6 RNA accumulates in neonates by non-specific uptake

Persistent detection of CR6 RNA in neonatal ilea and stool raised the possibility of prolonged transit time. Adult mice gavaged with Evans blue dye clear dye by 24 hours (Extended Data Fig. 7A)[24]. Conversely, neonates had visibly blue stool at 24 hours post-gavage and only cleared dye by 72 hours (Extended Data Fig. 7B), suggesting delayed transit time in neonates. However, since CR6 RNA was detectable up to 10dpi (Fig. 2C), reduced transit time did not fully explain prolonged shedding. Interestingly, wild-type neonatal ilea were visibly blue at 7dpi (Extended Data Fig. 7C), suggesting that the ileum retained inoculum. Enterocytes in the neonatal ileum internalize luminal material via non-specific endocytosis, a process which ceases by weaning[37,38]. We detected viral RNA in the epithelium of distal but not proximal small intestine of CR6-inoculated neonates (Fig. 6A,

Extended Data Fig. 8). These data suggest that viral inoculum is taken up, potentially via non-specific endocytosis, into neonatal ileal IECs.

Neonatal uptake of luminal material is mediated by endocytic machinery, including adapter protein DAB2[37]. Ileal *Dab2* expression was high at P6 and P13, but dropped by P21 (Fig. 6B), consistent with when neonatal ileal macromolecule uptake ceases in rodents[38]. Similarly, lysosomal enzyme N-acetylgalactosaminidase (*Naga*), involved in early-life macromolecule uptake[39], transcriptional repressor *Blimp1*/*Prdm1*, regulating intestinal maturation[39,40], and sucrase isomaltase (*Sis*), involved in transition to solid food consumption[39,40], exhibited a profound transition between P13 and P21 (Extended Data Fig. 7D-F).

In neonatal rats, treatment with the steroid cortisone acetate blocks non-specific uptake by driving premature maturation of the intestinal epithelium[41]. Cortisone treatment decreased ileal *Dab2* expression (Fig. 6B) and conferred adult-like expression of *Naga*, *Prdm1*, and *Sis* (Extended Data Fig. 7D-F), consistent with premature maturation of the neonatal mouse intestine. Ileal Evans blue retention was blocked by cortisone treatment (Extended Data Fig. 7C), and indeed, cortisone treatment of wild-type neonates decreased ileal CR6 RNA levels at 7dpi (Fig. 6C), although it did not affect stool viral RNA levels (Fig. 6D). Intriguingly, cortisone treatment of *Cd300lf*$^{-/-}$ neonates decreased both ileal and stool viral RNA at 7dpi, suggesting that a combinatorial effect of viral receptor and non-specific uptake or early infection may contribute to ongoing fecal shedding (Fig. 6E, F). Blocking virus uptake with cortisone treatment in wild-type neonates decreased ileal ISG expression at 1 and 7dpi (Fig. 6G, H), although whether this effect was secondary to decreased viral RNA or indirect immunosuppressive effects of steroids remains to be determined. Further, cortisone treatment increased serum anti-MNoV IgM and decreased anti-MNoV IgG, suggesting it may inhibit class switching and IgG responses to inoculum (Fig. 6I, J). Cortisone treatment of adult mice did not alter stool or tissue CR6 levels, suggesting that steroid administration does not modulate viral susceptibility independent of effects on neonatal non-specific uptake (Extended Data Fig. 9). These findings support that viral RNA in wild-type neonatal ilea is largely due to non-specific uptake of inoculum.

Discussion

Here, we discovered intriguing developmental differences contributing to dramatically changed outcomes between neonatal and juvenile or adult mice after inoculation with persistent MNoV. In early life, intact IFN signaling and an absence of tuft cells contribute to resistance to persistent MNoV. However, neonates retain viral RNA input in the absence of productive infection via non-specific endocytosis of inoculum by enterocytes.

Because fecal-oral transmission is the dominant means of interhost transmission for persistent MNoV, natural transmission from infected dams only after P16 is consistent with the lack of coprophagic behavior while pups rely exclusively on breastmilk. Indeed, cross-fostering pups of MNoV-infected dams to MNoV-naïve dams effectively eliminates litter infection[42]. If this natural transmission is bypassed by direct inoculation, however, distinct host factors in neonates promote viral RNA uptake but restrict productive infection.

Endocytosis in immature small intestinal enterocytes promotes early-life nutrient absorption, and early gut maturation delays growth and increases neonatal mortality[37,39,40]. Luminal material uptake also facilitates immune development, enabling passive immunity via transport of breastmilk antibodies, helping establish tolerance to food and microbial antigens[38]. However, our work demonstrates that pathogenic materials may also be taken up by endocytosis of luminal materials. Neonatal mice are highly susceptible to rotavirus until approximately P15-17, when gut closure occurs, and cortisone treatment of younger mice prior to inoculation decreases infection[43]. Thus, if permissive cells are available, passive uptake may facilitate neonatal infections. Conversely, early viral exposure induces innate and adaptive responses, raising the possibility that non-specific endocytosis protect against later infections. Juvenile mice represent an intriguing intermediate group, as they may experience non-specific endocytosis early in infection, but by 7dpi have undergone intestinal maturation. Future studies exploring the long-term immunological impact of juvenile infection may reveal how exposures throughout development influence adult immunity.

The persistence of viral RNA after clearance of infectious virus is recognized for numerous RNA viruses including measles virus and SARS-CoV-2. RNA persistence may complicate diagnosis, as viral RNA can be detected after infectious virions have cleared. Persistent RNA may also contribute to chronic immune activation, although its consequences have not been well-defined and may be pathogen- and site-specific[35]. Heightened IEC shedding in neonates may contribute to prolonged detection of fecal CR6 RNA.

Additional barriers limit neonatal CR6 infection despite passive inoculum uptake. Tuft cells, the target of CR6 in adults, are undetectable in our neonatal miceNon-epithelial cells also express CD300 molecules, though expression may vary between neonates and adults[44]. Our data support that without viral restriction by IFNs in hematopoietic cells, CR6 replicates in non-tuft cells in neonates, leading to viral dissemination and lethality. CR6 infection is more lethal in *Stat1*$^{-/-}$ neonates versus *Stat1*$^{-/-}$ adults[31,32]. Viral sensors like MDA5 and RIG-I are upregulated at weaning compared to early life[45], so *Stat1*-independent responses in adult mice may limit severe infection. Early-life endocytosis may also increase viral uptake compared to CD300LF-dependent infection alone. Alternatively, the microbiota enables CR6 infection in adult mice[24] and the neonatal gut microbiome composition is distinct from adults[46], so unique features of the neonatal *Stat1*$^{-/-}$ microbiota may increase infectivity.

Beyond increased lethality in *Stat1*$^{-/-}$ mice, the specific IFNs controlling CR6 are distinct in neonates versus adults. Type III IFNs control intestinal CR6 replication[15] while type I IFNs limit CR6 extraintestinal dissemination in adults[33]. In contrast, regulation of CR6-driven neonatal lethality is dominated by type I and II IFNs, although type III IFNs may also play a role. Involvement of different IFNs may reflect age-dependent tissue-specificity of IFN responses. In adults, IECs primarily express the type III IFN receptor[47], while neonatal IECs respond to both type I and III IFNs[48]. Multiple IFN classes may thus control viral replication and restrict systemic spread in neonates.

CD300LF plays a minor role in CR6 RNA uptake in wild-type neonates, as disrupting or blocking this receptor decreased viral RNA. Similarly, blocking virus replication with 2-CMC starting at 0dpi reduced viral RNA shedding, whereas treatment at 3dpi did not,

suggesting early replication. Interestingly, CD300LF has been implicated in facilitating cellular internalization of MNoV not via direct capsid binding but instead via interactions with phosphatidylserines[49] while shuttling vesicle-cloaked viral clusters into the endocytic pathway[50]. We found that cortisone reduced viral RNA shedding in *Cd300lf*$^{-/-}$ but not wild-type neonates. Thus, whether CD300LF itself could contribute to passive ileal absorption of virus in neonates remains an intriguing open question. CD300LF dependence is revealed in *Stat1*$^{-/-}$ neonates, as CD300LF is necessary for systemic spread[13]. Our work thus identifies numerous context-dependent host factors regulating viral RNA shedding in neonatal mice.

Despite children's high disease burden and important role in NoV transmission, host factors contributing to age-specific prolonged viral shedding are not well-defined. Host immunity limits NoV persistence, as immunocompromised patients of all ages experience extremely prolonged viral shedding[51]. Although anti-NoV antibodies accumulate with age, correlated with decreasing infection prevalence[52], antibody protection is limited in duration and against heterologous strains[3,53], so may not fully explain age-based differences. Innate immune regulation of NoV infection has not been well-studied in humans, although many aspects of innate immunity are immature in children[54]. Whether differences in immune control explain the variation in disease progression in young children is thus currently unclear. Our study points to both physiological and innate immune characteristics of neonates compared to juvenile or adult mice that regulate viral outcomes, highlighting the critical need to explore how developmental changes may govern infection responses.

Materials and Methods

Mice

Unless otherwise specified, C57BL/6J wild-type mice were originally purchased from Jackson Laboratories (JAX stock #000664, Bar Harbor, ME) and bred and housed in Washington University in Saint Louis (WUSTL) animal facilities under specific-pathogen-free, including MNoV-free, conditions. Animal protocols were approved by the Washington University Institutional Animal Care and Use Committee, protocol numbers 20160126, 20190162, 22-1040. Animals are housed up to five adult mice in a cage or a single dam with a lactating litter. The conditions in animal rooms used in this study fall within the standards set by the "Guide for the Care and Use of Laboratory Animals". Temperatures are maintained between 68-72°F and humidity between 30-70%. The room light cycle is 12h light, 12h dark. Age- and sex-matched adults were used in adult mouse infections. Litters of pups including males and females were used in neonatal mouse experiments. No statistical methods were used to pre-determine sample sizes but our sample sizes are similar to those reported in previous publications[19].

Knock-out mice on the C57BL/6J background were maintained in the same conditions and included the following strains: *Pou2f3*$^{-/-}$[32], *Cd300lf*$^{-/-}$[12], *Rag1*$^{-/-}$ (JAX stock #002216[55]), *Stat1*$^{-/-}$ (JAX stock #012606[56]), *Ifnar1*$^{-/-}$[57], *Ifngr1*$^{-/-}$ (JAX stock #003288[58]) and *Ifnlr1*$^{-/-}$[14]. *Ifnar1*$^{-/-}$*Ifngr1*$^{-/-}$ mice were generated by crossing *Ifnar1*$^{-/-}$ and *Ifngr1*$^{-/-}$ mice.

Stat1 conditional knockout mice were generated by crossing *Stat1*$^{f/f}$ mice (MMRRC stock #32054[59]) to the following Cre lines: *Villin-Cre* (JAX stock #:004586[60]), *Lysm-Cre* (JAX stock #004781[61]), and *Vav-iCre* (JAX stock #008610[62,63]). All infections were performed on Cre+ and Cre− littermates born to Cre− dams. *Vav-iCre* pups were screened for germline deletion of the floxed allele.

Cd300lf$^{-/-}$ *CD300ld*$^{-/-}$ mice were generated by co-injecting gRNAs targeting the *CD300lf* and *Cd300ld* loci into C57BL/6J fertilized zygotes along with Cas9 mRNA. A founder mouse with the following mutations was recovered:

Cd300lf locus –	WT: CGATATACCTCA–GGCTGGAAGGAT
	KO: CGATATACCTCAAGGCTGGAAGGAT
Cd300ld locus –	WT: TATTCCTCATAC–TGGAAGGGTTAC
	KO: TATTCCTCATACGTGGAAGGGTTAC

Additional generations were genotyped by Transnetyx (Cordova, TN) from tail biopsy specimens using real-time PCR with mutation-specific probes.

For comparison of pups by vendor source (**Fig. S1A**), C57BL/6 mice were bred at WUSTL, or purchased as lactating dams with litters from Jackson Laboratories (JAX stock #000664) or Charles River (CR stock #027). For comparison of pups by genetic background (**Fig. S1B**), C57BL/6 (#000664), BALB/c (#000651), A/J (#000646), NOD (#001976), and 129S1 (#002448) lactating dams with litters were purchased from JAX. PWK/PhJ (#003715) adults were purchased from JAX and bred at WUSTL due to a lack of availability of lactating dams for this strain. For comparison of C57BL/6 and BALB/c pups (**Fig. S1C, D**), lactating dams with litters were purchased from CR (CR stock #027 and #028, respectively). For comparison of C57BL/6 and BALB/c adults (**Fig. S1E, F**), 6-week-old adults were purchased from CR (CR stock #027 and #028, respectively).

Generation of viral stocks

Stocks of MNoV strain CR6 were generated from molecular clones as previously described[13]. Briefly, plasmids encoding the viral genomes were transfected into 293T cells to generate infectious virus, which was subsequently passaged on BV2 cells. After two passages, BV2 cultures were frozen and thawed to liberate virions. Virus was concentrated by centrifugation in a 100,000 MWCO ultrafiltration unit (Vivaspin, Sartorius). Titers of virus stocks were determined by plaque assay on BV2 cells.

MNoV infections and sample collection

For adult MNoV infections, 6–9-week-old mice were orally inoculated with 1e6 plaque-forming units (PFU) of CR6 in a volume of 25µl. For neonatal and juvenile infections, postnatal day (P)6 and P15 mice, respectively, were gavaged with 10^6 PFU of CR6 in a volume of 50µl using a 22ga plastic feeding tube. Virus stocks contained a range of $10^{7.4}$-$10^{7.7}$ genome copies in 10^6 PFU. Stool samples were collected by gently palpating the abdomen to encourage defecation. Given the challenge of collecting stool from young

mice, stool was collected as possible, and the number of samples collected was generally representative of a much greater number of mice. Tissues were collected from mice at time of euthanasia or shortly after natural death when tissues were still intact. Stool and tissues were harvested into 2-ml tubes (Sarstedt, Germany) with 1-mm-diameter zirconia/silica beads (Biospec, Bartlesville, OK). Samples were frozen and stored at −80C until RNA extraction or plaque assay. For controls for treatment groups, infected groups include mice treated with PBS or PBS containing 2% Tween-80.

RNA extraction and quantitative reverse transcription-PCR

As previously described[14], RNA was isolated from stool using a ZR-96 Viral RNA kit (Zymo Research, Irvine, CA) according to the manufacturer's protocol. RNA from tissues was isolated using TRI Reagent with a Direct-zol-96 RNA kit (Zymo Research, Irvine, CA) according to the manufacturer's protocol. 5μl of RNA from stool or tissue was used for cDNA synthesis with the ImPromII reverse transcriptase system (Promega, Madison, WI). MNoV TaqMan assays were performed, using a standard curve for determination of absolute viral genome copies. PrimeTime qPCR assays were used for *Cd300lf* (Mm.PT.58.13995989), *Ifit1* (Mm.PT.58.32674307), *Mx2* (Mm.PT.58.11386814) using a standard curve. SYBR green PCR was performed for *Dab2* (Fw 5'-TCATCAAACCCCTCTGTGGT, Rv 5'-AGCGAGGACAGAGGTCAACA), *Naga* (Fw 5'- TGCCTTCCTAGCTGACTATGC, Rv 5'- GTCATTTTGCCCATGTCCTC), *Prdm1* (Fw 5'- AGTTCCCAAGAATGCCAACA, Rv 5'- TTTCTCCTCATTAAAGCCATCAA), *Sis* (Fw 5'- TGCCTGCTGTGGAAGAAGTAA, Rv 5'- CAGCCACGCTCTTCACATTT) using Power SYBR Green master mix (Applied Biosystems). qPCR for housekeeping gene *Rps29* was performed as previously described[14]. All samples were analyzed with technical duplicates.

MNoV-specific ELISA

CR6 at a concentration of 5e6 PFU/well diluted in PBS was used to coat a 96-well MaxiSorp plate overnight at 4°C. Two-fold serial dilutions of mouse IgG (Sigma-Aldrich, I5381, starting at 12.5ng/ml) or mouse IgM (Sigma-Aldrich, PP50, starting at 250ng/ml) were used to coat overnight as standard controls. Wells were washed three times with wash buffer (0.05% Tween-20 in PBS) between each incubation. After one hour of blocking with 1% BSA in PBS (blocking buffer), serum diluted 1:50 in blocking buffer was incubated for 2 hours. After washing, anti-mouse IgG-HRP (Sigma-Aldrich, A3673, 1:2000 dilution in blocking buffer) or anti-mouse IgM-HRP (Sigma-Aldrich, A8786, 1:2000 dilution in blocking buffer) was incubated for two hours. After washing, ELISA TMB Substrate solution (eBioscience, San Diego, CA) was added, and the reaction stopped with the addition of stop solution (2N H_2SO_4). OD was read at 450nm and reference wavelength 570nm and concentration of samples determined against the standard curve.

RNA-in situ hybridization

Ilea and colons were collected, and intestinal contents flushed with 10% neutral buffered formalin (NBF). Tissues were Swiss-rolled and fixed overnight in 10% NBF at 4°C, washed three times with 70% ethanol, and embedded in paraffin. RNAscope assays were performed using RNAscope Multiplex Fluorescent v2 assays (ACD) according to manufacturer's

instructions. Briefly, 5μm sections were baked at 60°C for one hour, then deparaffinized by washing with xylenes and 100% ethanol. Antigen retrieval was performed by boiling sections in Target Retrieval Reagent (ACD) for 15 minutes, followed by 30 minutes of treatment with Protease Plus (ACD) at 40°C. Tissues were hybridized with a custom-designed probe to MNoV strain CR6 RNA, and in some experiments a probe against *Epcam* (418151, ACD) for 2 hours at 40°C, followed by amplification and development of channel-specific signals according to manufacturer's protocol, and staining with DAPI to visualize nuclei. Positive- and negative-control probes were included to validate staining protocols. Images were acquired using an AxioScan Z1 (Zeiss) slide scanner and ImageJ (Version 2.9.0) was used to analyze the images.

Immunofluorescent staining

Ilea and colon sections were Swiss rolled and paraffin embedded as described above. Staining for DCLK1 and NS6/7 was generally performed as described previously [10]. Briefly, 5μm sections were deparaffinized by washing three times, 5 minutes each, in xylenes and isopropanol, followed by 5 minutes in running water and 5 minutes in Tris buffered saline with 0.1% Tween-20 (TBST). Antigen retrieval was performed by boiling for 10 minutes in Antigen Unmasking solution (Vector) followed by washing 5 minutes in TBST. Blocking was performed in 1% bovine serum albumin and 10% goat serum in TBST for 30 minutes at room temperature. When staining for dsRNA, an additional 1 hour blocking with F(ab) fragment anti-mouse IgG (ab6668, Abcam, 0.1mg/ml) was performed. Primary staining was performed overnight at 4°C, using rabbit anti-DCLK1 (D2U3L, Cell Signaling, 1:300), guinea pig anti-NS6/7 (1:1000, gift of Kim Green), and mouse anti-dsRNA (rJ2, MilliporeSigma, 1:200). Samples were washed in TBST, followed by secondary staining for 1 hour at room temperature with goat anti-rabbit AlexaFluor 488 (A11008, Invitrogen, 1:500), goat anti-guinea pig AlexaFluor 647 (A21450, Invitrogen, 1:500), and goat anti-mouse AlexaFluor 555 (A21425, Invitrogen, 1:500). Samples were washed in TBST, counterstained with DAPI (1:1000), and mounted with Fluorshield mounting media. Tuft cells were quantified as DCLK1-positive cells per crypt/villus, counting at least 50 crypts/villi per mouse, beginning at the distal end of the ileum and the proximal end of the colon.

Plaque assay

For CR6 plaque assays, BV2 cells were seeded at 2e6 cells/well in a 6 well plate and grown overnight. Tissues were weighed and samples homogenized by bead beating in 500μl DMEM. Sample were spun at 2500g for 3 minutes at 4°C, then supernatant removed and incubated for one hour at room temperature with rocking. 10-fold dilutions were prepared and applied to each well of BV2 cells, followed by one hour of incubation at room temperature with gentle rocking. Inoculum was removed and 2ml of overlay media added (MEM, 10% FBS, 2mM L-Glutamine, 10 mM HEPES, and 1% methylcellulose). Plates were incubated for 72 hours prior to visualization after crystal violet staining (0.2% crystal violet and 20% ethanol).

Fc-CD300lf blocking

CR6 neutralization was assessed *in vitro* by measuring cytotoxicity. 2e4 BV2 cells/well were plated in a 96 well plate. CR6 was incubated with dilutions of the Fc region of murine IgG2b

fused to the human CD300LF ectodomain[13] or mouse CD300LF ectodomain[30] for one hour at 37°C and used to infect BV2 cells at an MOI of 0.05. Plates were incubated at 37°C for 48 hours, then 25μl of CellTiter Glo (Promega) added per well and luminescence measured to quantify viability via cellular ATP concentrations. Assays were performed in triplicate.

For neutralization with Fc-fusion proteins *in vivo*, 1e6 PFU CR6 was incubated with 1.17μg of human or mouse Fc-CD300lf in 50μl media for one hour at 37°C prior to oral infection as described above.

Mouse treatments

Cortisone acetate (Sigma, C3130) was dissolved 25mg/ml in PBS containing 2% Tween-80 at 37°C and vortexed to make a fine suspension before injection. Mice were treated by subcutaneous injection of 0.5mg/g body weight[41] or the equivalent volume of vehicle using a 31ga (neonates) or 28ga (adults) needle to inject into the scruff. Cortisone acetate reduced weight gain and variably contributed to death in pups, likely due to reduced nutrient absorption after premature gut maturation.

2-C-Methylcytidine (2-CMC; Neta Scientific, AST-F12743) was dissolved 20mg/ml into PBS. Mice were treated by subcutaneous injection of 100mg/kg body weight[34] or the equivalent volume of vehicle using a 31ga needle to inject into the scruff daily.

For intestinal transit time assessment, mice were gavaged with 50μl (neonates) or 400μl (adults) of a 1% Evans blue solution. Fecal pellets were resuspended in PBS and intestines were collected from neonatal mice for assessment of blue color.

Statistical analysis

Data were analyzed with Prism 9 software (GraphPad Software). In all graphs, ns indicates not significant ($p > 0.05$); * $p < 0.05$; ** $p < 0.01$; *** $p < 0.001$; **** $p < 0.0001$. Data were tested for normal distribution using Shapiro-Wilk tests and non-parametric tests performed if data were not normally distributed. F tests or Brown Forsythe tests were performed to confirm equal variances between groups. No statistical method was used to predetermine sample size. No data were excluded from the analyses. When possible, littermate controls were randomized to groups to minimize weight variability between groups. The Investigators were not blinded to allocation during experiments and outcome assessment except for tuft cell quantification, which was performed blinded to sample source.

Materials availability: All reagents are available from M.T.B. under a material transfer agreement with Washington University.

Extended Data

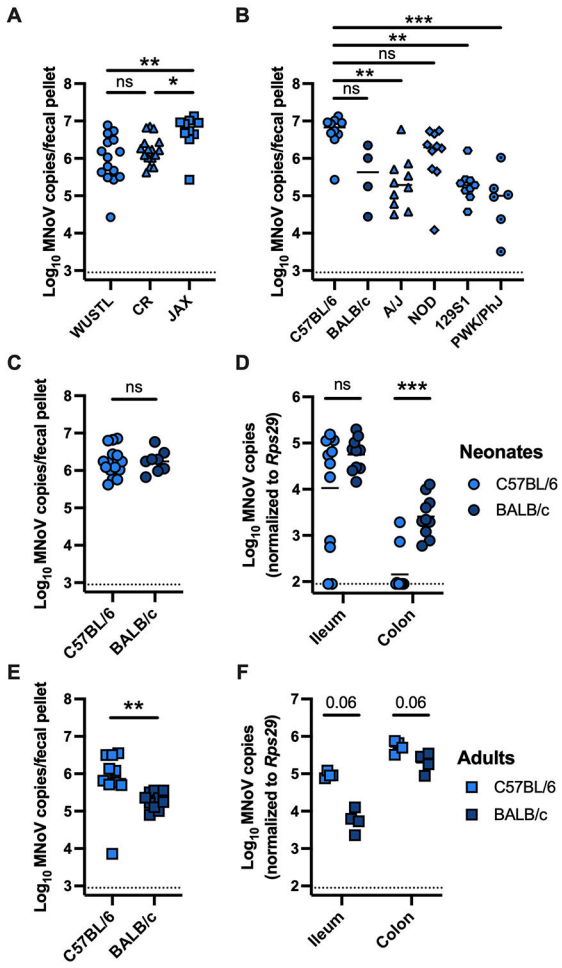

Extended Data Fig. 1. Source and genetic background of mice influences persistent MNoV shedding as neonates and adults.

(A) C57BL/6 neonates bred at Washington University in St. Louis (WUSTL), Charles River (CR), or Jackson Laboratories (JAX) were orally inoculated with CR6 at P6 and MNoV genome copies detected in 7dpi stool samples by qPCR. **(B)** Neonates on the indicated backgrounds, all sourced from JAX, were orally inoculated with CR6 at P6 and MNoV genome copies detected in 7dpi stool samples by qPCR. **(C, D)** Neonates on the indicated background, sourced from CR, were orally inoculated with CR6 at P6 and MNoV genome copies detected in 7dpi samples by qPCR in stool **(C)** and tissues **(D)**. **(E, F)** Adult mice on the indicated background, sourced from CR, were orally inoculated with CR6 and MNoV genome copies detected in 10dpi samples by qPCR in stool **(E)** and tissues **(F)**. Analyzed by Kruskal-Wallis test with Dunn's multiple comparisons test **(A, B)**, two-tailed t-test (**C)** two-tailed Mann-Whitney test **(D-F)** corrected with the Holm-Šídák method **(D, F)**. **(A)** WUSTL (n=15, 4 litters), CR (n=16, 3 litters), JAX (n=10, 2 litters), *p=0.0427, **p=0.0037. **(B)** C57Bl/6 (n=10, 2 litters), BALB/c (n=4, 2 litters), A/J (n=10, 3 litters), NOD (n=10, 3 litters), 129S1 (n=9, 2 litters), PWK/PhJ (n=6, 2 litters), **p=0.0023 (C57BL/6 vs. A/J), **p=0.0012 (C57BL/6 vs. 129S1), ***p=0.0003. **(C)** C57Bl/6 (n=16, 3 litters), BALB/c

(n=8, 2 litters). **(D)** C57Bl/6 (n=12, 2 litters), BALB/c (n=10, 2 litters). ***p=0.0001. **(E)** N=10 mice per group from 2 independent experiments, **p=0.0015. **(F)** N=4 mice per group from one experiment, p=0.0563 (ileum), p=0.0571 (colon). Dashed lines indicate limit of detection for assays. ns, not significant (p>0.05).

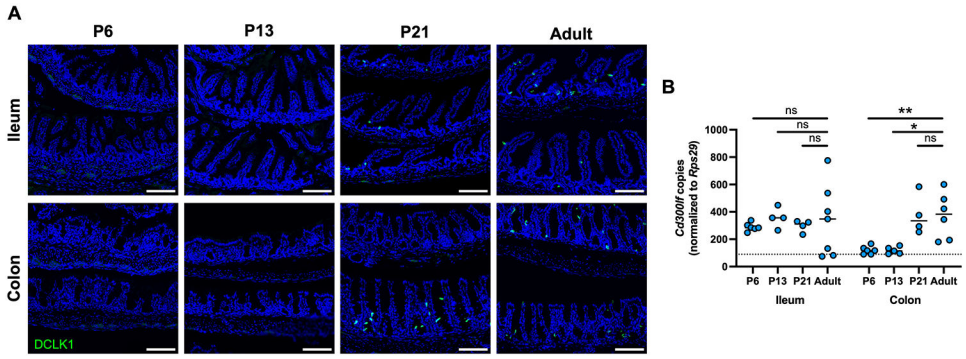

Extended Data Fig. 2. Tuft cells and *Cd300lf* expression in early life.

(A) Representative images of tuft cells quantified by immunofluorescent staining of DCLK1 in naïve C57BL/6 mice (quantified data shown in Fig. 3C). **(B)** *Cd300lf* was quantified in intestinal samples from naïve C57BL/6 mice by qPCR at the indicated timepoints. P6 (n=6, 1 litter), P13 (n=4, 2 litters), P21 (n=4, 2 litters), adult (n=7, 2 experiments), analyzed by Kruskal-Wallis test with Dunn's multiple comparisons test. *p=0.0183, **p=0.0087. Dashed lines indicate limit of detection for assay. ns, not significant (p>0.05).

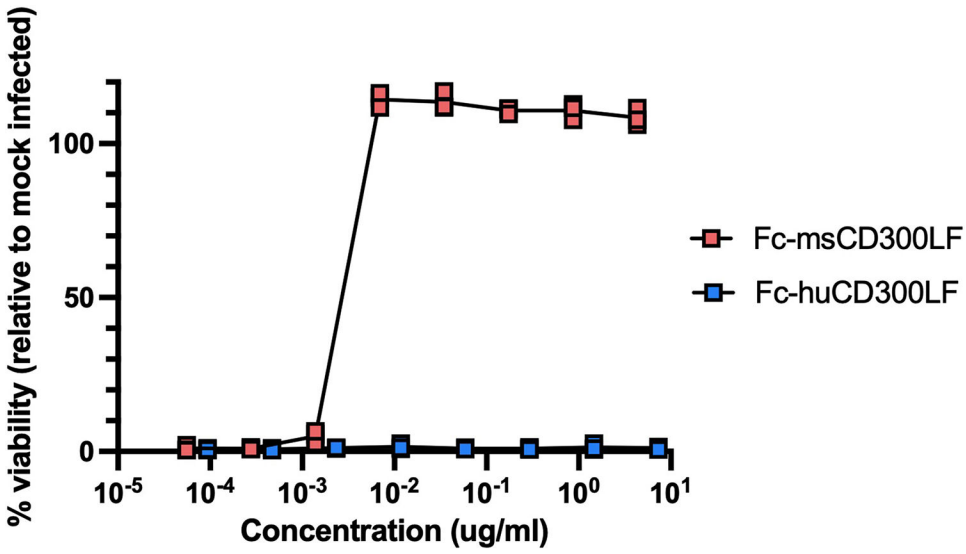

Extended Data Fig. 3. Mouse but not human Fc-CD300LF blocks CR6 infection in vitro.

CR6 was incubated with Fc-fusion proteins with either the human or mouse CD300LF ectodomains for 1 hour at 37C, prior to infection of BV2 cells at an MOI of 0.05. Cell viability was measured by CellTiter Glo 48 hours post-infection. 3 technical replicates from a single experiment.

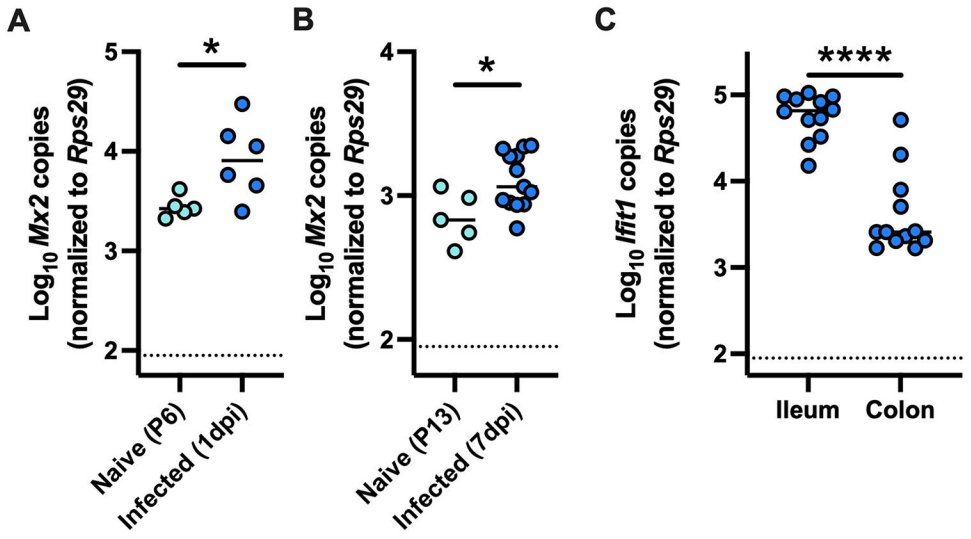

Extended Data Fig. 4. CR6 induces ISG expression in the ileum.

Wild-type neonates were orally inoculated with CR6 at P6. *Mx2* was quantified by qPCR from ilea collected at 1 dpi **(A)** or 7 dpi **(B)** and compared to naïve neonates. **(C)** *Ifit1* expression was quantified in the ileum and colon of CR6-inoculated neonates at 7dpi. **(A)** Naïve (n=5, 1 litter), infected (n=6, 3 litters), analyzed by Welch's two-tailed t-test, *p=0.0289. **(B)** Naïve (n=5, 2 litters), infected (n=13, 4 litters), analyzed by two-tailed t-test, **p=0.0188. **(C)** N=12 pups from 2 litters sourced from Charles River, analyzed by two-tailed Mann-Whitney test, ****p<0.0001.

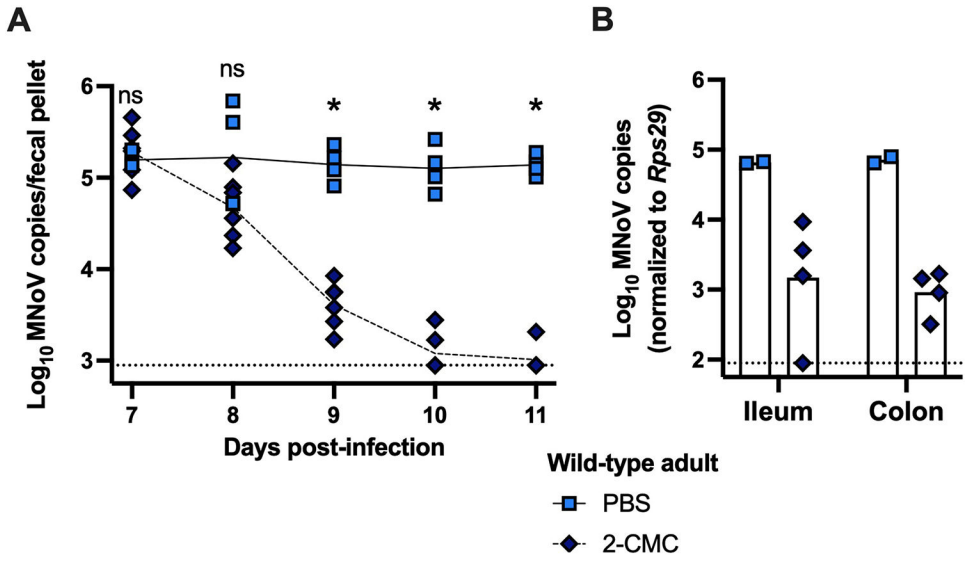

Extended Data Fig. 5. 2-CMC blocks CR6 shedding in wild-type adult mice.

Wild-type adult mice were orally inoculated with CR6. 100mg/kg 2-CMC or PBS were injected subcutaneously daily at 7-9dpi. Stool was collected from 7-11dpi **(A)** and tissues at 11dpi **(B)**, and MNoV genome copies quantified by qPCR. **(A)** PBS (n=4), 2-CMC (n=6), from two experiments. Analyzed by two-tailed Mann-Whitney test corrected with the Holm-Šídák method, *p=0.0376 (9dpi, 10dpi), *p=0.0236 (11dpi). **(B)** PBS (n=2), 2-CMC

(n=4), from one experiment. Dashed lines indicate limit of detection for assays. ns, not significant.

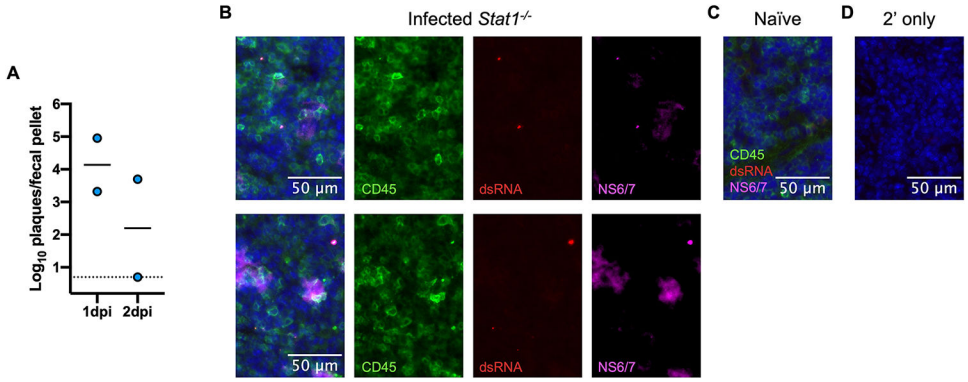

Extended Data Fig. 6. CR6 replicates in the spleens of *Stat1*$^{-/-}$ neonates.

(A) Wild-type neonates (P6) were orally inoculated with CR6. Infectious virus from 1-2dpi stool was quantified by plaque assay on BV2 cells. n=2 stools collected per time point. **(B)** Additional replicates of spleens from CR6-inoculated *Stat1*$^{-/-}$ neonates, stained as in Fig. 5J. **(C)** Spleen from a naïve neonate stained as in Fig. 5J. **(D)** 2' only antibody control for spleen in Fig. 5J.

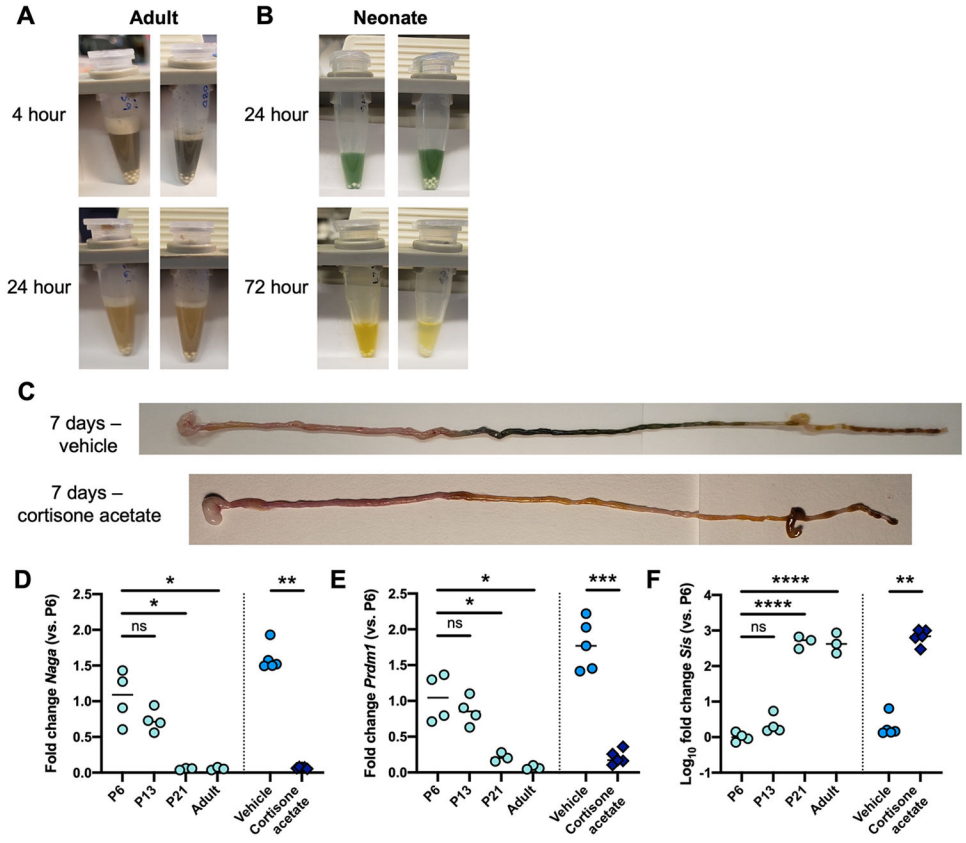

Extended Data Fig. 7. Evans blue dye is retained in the distal small intestine of neonatal mice.

(A) Adult mice were gavaged with 400ul Evans blue dye and stool collected at 4- and 24-hours post-gavage. **(B)** Neonates were gavaged at P6 with 50ul Evans blue dye and stool collected at 24- and 72-hours post-gavage. Stool was resuspended in PBS for assessment of blue color. Representative of 3 adults from one experiment and 8 neonates from three litters. **(C)** Neonates were gavaged at P6 with 50ul Evans blue dye and treated with 0.5mg/g cortisone acetate or vehicle. Intestines were collected at 7dpi post-gavage and assessed for blue color across the length of the intestines. Representative of 3 cortisone acetate and 3 vehicle-treated neonates from two litters. **(D-F)** Ileal samples were collected from naïve mice at P6, P13, P21, and as adults (left) or at 7dpi (P13) from littermates inoculated with CR6 and treated subcutaneously with 0.5mg/g cortisone acetate or vehicle at P6 (right). *Naga* **(D)**, *Prdm1* **(E)**, and *Sis* **(F)** expression was quantified by qPCR. P6 (n=4,1. litter), P13 (n=4, 2 litters), P21 (n=3, 2 litters), adult (n=3, 1 experiment), 7dpi cortisone acetate (n=5, 2 litters), 7dpi vehicle (n=5, 2 litters). Naïve time course analyzed by Welch's ANOVA test with Dunnett's T3 multiple comparisons test (**D, E,** time course), ANOVA with Dunnett's multiple comparisons test **(F**, time course**),** two-tailed Mann-Whitney test **(D, F,** vehicle vs. cortisone acetate), or Welch's two-tailed t-test **(E**, vehicle vs cortisone acetate). **(D)** *p=0.0295 (P6 vs. P21), *p=0.0298 (P6 vs. adult), **p=0.0079 (vehicle vs. cortisone acetate). **(E)** *p=0.0399 (P6 vs. P21), *p=0.0245 (P6 vs. adult), ***p=0.0003 (vehicle vs. cortisone acetate). **(F)** ****p<0.0001 (P6 vs. P21, P6 vs. adult), **p=0.0079 (vehicle vs. cortisone acetate). ns, not significant (p>0.05).

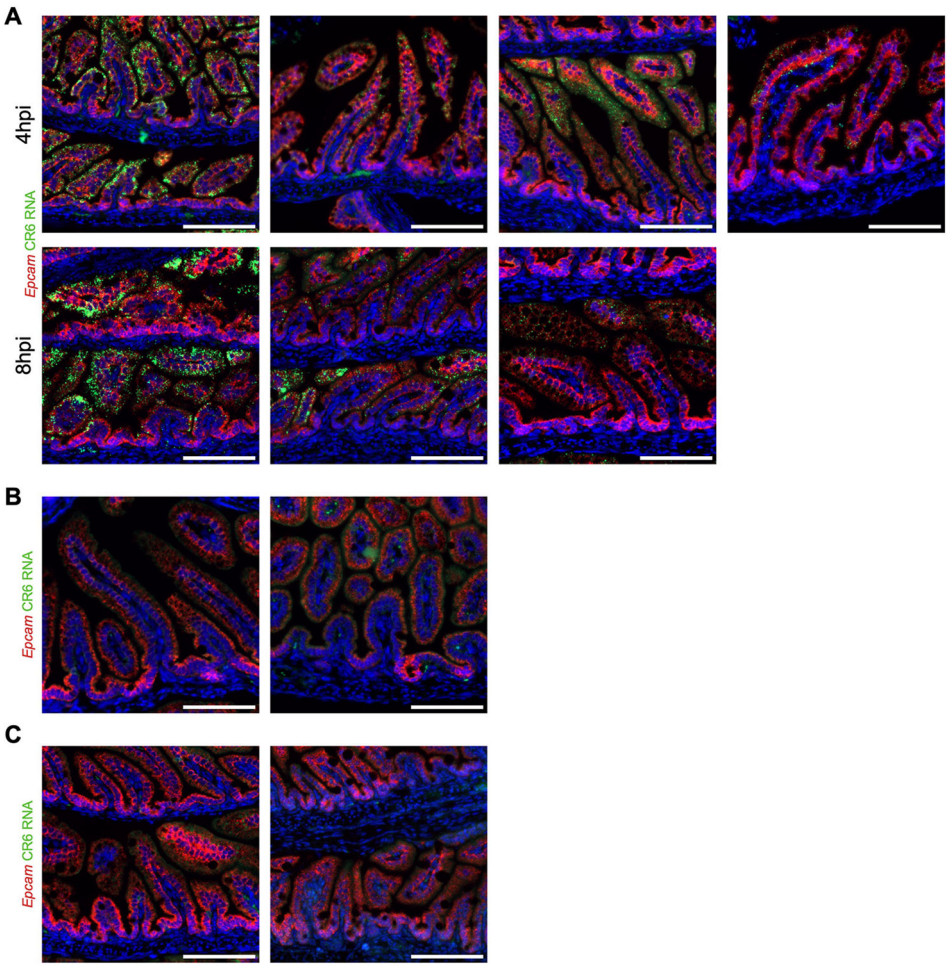

Extended Data Fig. 8. CR6 uptake is localized to the distal small intestine.

Ilea stained for Epcam and CR6 RNA. All replicates collected are shown. (**A**) Additional replicates of distal small intestinal sections from neonates inoculated with CR6 at P6, collected at 4 or 8hpi. (**B**) Proximal small intestinal sections collected at 8hpi. (**C**) Distal small intestinal sections from naïve neonates. Scale bars are 100μm long.

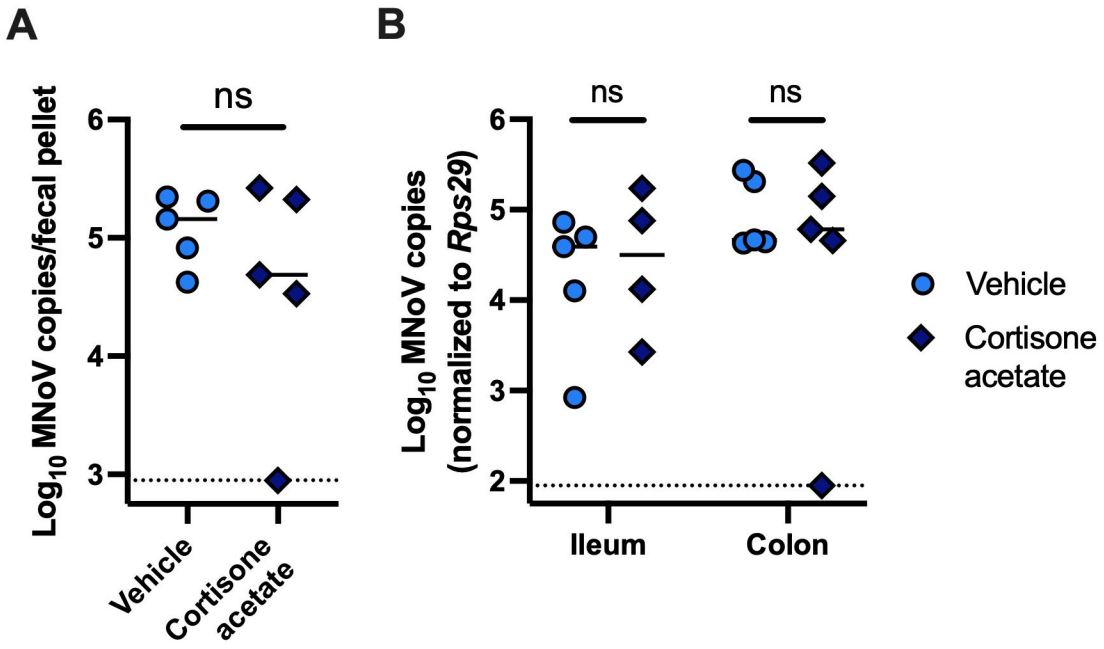

Extended Data Fig. 9. Cortisone acetate treatment does not affect CR6 infection in adult mice.

Wild-type adult mice were orally inoculated with CR6 and treated subcutaneously with 0.5mg/g cortisone acetate or vehicle. Stool **(A)** and tissue **(B)** virus levels were quantified by qPCR at 7dpi. Vehicle (n=5) and cortisone acetate (n=5), from two independent experiments. Analyzed by Welch's two-tailed t-test **(A)** and two-tailed Mann-Whitney test corrected with the Holm-Šídák method **(B)**. Dashed lines indicate limit of detection for assays. ns, not significant.

Supplementary Material

Refer to Web version on PubMed Central for supplementary material.

Acknowledgments:

We acknowledge all members of the Baldridge laboratory for helpful discussions, and specifically Hongju Deng and Lynne Foster for assistance with mouse colony maintenance. We are grateful to Robert Orchard (University of Texas Southwestern Medical Center) for providing Fc-CD300lf complexes.

Funding:

This work was supported by the National Institutes of Health (NIH) grants R01AI141478 (S.M.K., M.T.B.), R01AI139314 and R01AI127552 (M.T.B.), R01A1148467 (C.B.W.), F31AI167499-01 (E.A.K.), as well as the Burroughs Wellcome Fund (C.B.W.), National Science Foundation DGE-1745038/DGE-2139839 (E.A.K.), and the Pew Biomedical Scholars Program of the Pew Charitable Trusts (M.T.B.). The funders had no role in study design, data collection and analysis, decision to publish, or preparation of the manuscript.

Data availability:

The data from this study are tabulated in the main paper and extended materials. Source data are provided with this paper.

References

1. Grytdal SP et al. Incidence of Norovirus and Other Viral Pathogens That Cause Acute Gastroenteritis (AGE) among Kaiser Permanente Member Populations in the United States, 2012-2013. PLoS One 11, e0148395 (2016). [PubMed: 27115485]
2. Cannon JL, Lopman BA, Payne DC & Vinjé J Birth Cohort Studies Assessing Norovirus Infection and Immunity in Young Children: A Review. Clin. Infect. Dis 69, 357–365 (2019). [PubMed: 30753367]
3. Saito M. et al. Multiple norovirus infections in a birth cohort in a Peruvian Periurban community. Clin. Infect. Dis 58, 483–91 (2014). [PubMed: 24300042]
4. Shioda K. et al. Can Use of Viral Load Improve Norovirus Clinical Diagnosis and Disease Attribution? Open forum Infect. Dis 4, ofx131 (2017). [PubMed: 32455144]
5. Simmons K., Gambhir M, Leon J & Lopman B Duration of immunity to norovirus gastroenteritis. Emerg. Infect. Dis 19, 1260–7 (2013). [PubMed: 23876612]
6. Baldridge MT, Turula H & Wobus CE Norovirus Regulation by Host and Microbe. Trends Mol. Med 22, 1047–1059 (2016). [PubMed: 27887808]
7. Grau KR et al. The major targets of acute norovirus infection are immune cells in the gut-associated lymphoid tissue. Nat. Microbiol 2, 1586–1591 (2017). [PubMed: 29109476]
8. Graziano VR et al. CD300lf Conditional Knockout Mouse Reveals Strain-Specific Cellular Tropism of Murine Norovirus. J. Virol 95, 1–14 (2020).
9. Nice TJ, Strong DW, McCune BT, Pohl CS & Virgin HW A single-amino-acid change in murine norovirus NS1/2 is sufficient for colonic tropism and persistence. J. Virol 87, 327–34 (2013). [PubMed: 23077309]
10. Wilen CB et al. Tropism for tuft cells determines immune promotion of norovirus pathogenesis. Science 360, 204–208 (2018). [PubMed: 29650672]
11. Haga K. et al. Functional receptor molecules CD300lf and CD300ld within the CD300 family enable murine noroviruses to infect cells. Proc. Natl. Acad. Sci 113, E6248–E6255 (2016). [PubMed: 27681626]
12. Orchard RC et al. Discovery of a proteinaceous cellular receptor for a norovirus. Science 353, 933–6 (2016). [PubMed: 27540007]
13. Graziano VR et al. CD300lf is the primary physiologic receptor of murine norovirus but not human norovirus. PLoS Pathog. 16, e1008242 (2020). [PubMed: 32251490]
14. Baldridge MT et al. Expression of Ifnlr1 on Intestinal Epithelial Cells Is Critical to the Antiviral Effects of Interferon Lambda against Norovirus and Reovirus. J. Virol 91, e02079–16 (2017). [PubMed: 28077655]
15. Nice TJ et al. Interferon-λ cures persistent murine norovirus infection in the absence of adaptive immunity. Science 347, 269–73 (2015). [PubMed: 25431489]
16. Nice TJ et al. Type I Interferon Receptor Deficiency in Dendritic Cells Facilitates Systemic Murine Norovirus Persistence Despite Enhanced Adaptive Immunity. PLoS Pathog. 12, e1005684 (2016). [PubMed: 27327515]
17. Grau KR et al. The intestinal regionalization of acute norovirus infection is regulated by the microbiota via bile acid-mediated priming of type III interferon. Nat. Microbiol 5, 84–92 (2020). [PubMed: 31768030]
18. Thackray LB et al. Critical Role for Interferon Regulatory Factor 3 (IRF-3) and IRF-7 in Type I Interferon-Mediated Control of Murine Norovirus Replication. J. Virol 86, 13515–13523 (2012). [PubMed: 23035219]
19. Roth AN et al. Norovirus infection causes acute self-resolving diarrhea in wild-type neonatal mice. Nat. Commun 11, (2020).
20. Helm EW et al. Environmentally-triggered contraction of the norovirus virion determines diarrheagenic potential. Front. Immunol 13, 1043746 (2022). [PubMed: 36389732]
21. Ebino KY Studies on coprophagy in experimental animals. Jikken Dobutsu. 42, 1–9 (1993). [PubMed: 8462627]

22. Rasmussen TS et al. Mouse Vendor Influence on the Bacterial and Viral Gut Composition Exceeds the Effect of Diet. Viruses 11, 0–14 (2019).
23. Hildebrand F. et al. Inflammation-associated enterotypes, host genotype, cage and inter-individual effects drive gut microbiota variation in common laboratory mice. Genome Biol. 14, R4 (2013). [PubMed: 23347395]
24. Baldridge MT et al. Commensal microbes and interferon-λ determine persistence of enteric murine norovirus infection. Science 347, 266–9 (2015). [PubMed: 25431490]
25. Blutt SE, Warfield KL, O'Neal CM, Estes MK & Conner ME Host, viral, and vaccine factors that determine protective efficacy induced by rotavirus and virus-like particles (VLPs). Vaccine 24, 1170–1179 (2006). [PubMed: 16191453]
26. Gerbe F. et al. Intestinal epithelial tuft cells initiate type 2 mucosal immunity to helminth parasites. Nature 529, 226–230 (2016). [PubMed: 26762460]
27. Saqui-Salces M. et al. Gastric tuft cells express DCLK1 and are expanded in hyperplasia. Histochem. Cell Biol 136, 191–204 (2011). [PubMed: 21688022]
28. Schneider C. et al. A Metabolite-Triggered Tuft Cell-ILC2 Circuit Drives Small Intestinal Remodeling. Cell 174, 271–284.e14 (2018). [PubMed: 29887373]
29. Haber AL et al. A single-cell survey of the small intestinal epithelium. Nature 551, 333–339 (2017). [PubMed: 29144463]
30. Nelson CA et al. Structural basis for murine norovirus engagement of bile acids and the CD300lf receptor. Proc. Natl. Acad. Sci. U. S. A 115, E9201–E9210 (2018). [PubMed: 30194229]
31. Strong DW, Thackray LB, Smith TJ & Virgin HW Protruding Domain of Capsid Protein Is Necessary and Sufficient To Determine Murine Norovirus Replication and Pathogenesis In Vivo. J. Virol 86, 2950–2958 (2012). [PubMed: 22258242]
32. Walker FC et al. Norovirus evolution in immunodeficient mice reveals potentiated pathogenicity via a single nucleotide change in the viral capsid. PLoS Pathog. 17, e1009402 (2021). [PubMed: 33705489]
33. Hwang S. et al. Nondegradative role of Atg5-Atg12/Atg16L1 autophagy protein complex in antiviral activity of interferon gamma. Cell Host Microbe 11, 397–409 (2012). [PubMed: 22520467]
34. Rocha-Pereira J, Van Dycke J & Neyts J Treatment with a Nucleoside Polymerase Inhibitor Reduces Shedding of Murine Norovirus in Stool to Undetectable Levels without Emergence of Drug-Resistant Variants. Antimicrob. Agents Chemother 60, 1907–11 (2015). [PubMed: 26711754]
35. Griffin DE Why does viral RNA sometimes persist after recovery from acute infections? PLoS Biol. 20, e3001687 (2022). [PubMed: 35648781]
36. Zhang Z. et al. IL-22-induced cell extrusion and IL-18-induced cell death prevent and cure rotavirus infection. Sci. Immunol 5, (2020).
37. Park J. et al. Lysosome-Rich Enterocytes Mediate Protein Absorption in the Vertebrate Gut. Dev. Cell 51, 7–20.e6 (2019). [PubMed: 31474562]
38. Weström B, Arévalo Sureda E, Pierzynowska K, Pierzynowski SG & Pérez-Cano F-J The Immature Gut Barrier and Its Importance in Establishing Immunity in Newborn Mammals. Front. Immunol 11, 1153 (2020). [PubMed: 32582216]
39. Harper J, Mould A, Andrews RM, Bikoff EK & Robertson EJ The transcriptional repressor Blimp1/Prdm1 regulates postnatal reprogramming of intestinal enterocytes. Proc. Natl. Acad. Sci. U. S. A 108, 10585–90 (2011). [PubMed: 21670299]
40. Muncan V. et al. Blimp1 regulates the transition of neonatal to adult intestinal epithelium. Nat. Commun 2, 452 (2011). [PubMed: 21878906]
41. Daniels VG, Hardy RN, Malinowska KW & Nathanielsz PW The influence of exogenous steroids on macromolecule uptake by the small intestine of the new-born rat. J. Physiol 229, 681–95 (1973). [PubMed: 4735058]
42. Compton SR Prevention of Murine Norovirus Infection in Neonatal Mice by Fostering. J. Am. Assoc. Lab. Anim. Sci. 47, 25–30 (2008).

43. Wolf JL, Cukor G, Blacklow NR, Dambrauskas R & Trier JS Susceptibility of mice to rotavirus infection: effects of age and administration of corticosteroids. Infect. Immun 33, 565–74 (1981). [PubMed: 6268547]
44. Zenarruzabeitia O. et al. The expression and function of human CD300 receptors on blood circulating mononuclear cells are distinct in neonates and adults. Sci. Rep 6, 32693 (2016). [PubMed: 27595670]
45. Pott J. et al. Age-dependent TLR3 expression of the intestinal epithelium contributes to rotavirus susceptibility. PLoS Pathog. 8, e1002670 (2012). [PubMed: 22570612]
46. Al Nabhani Z. et al. A Weaning Reaction to Microbiota Is Required for Resistance to Immunopathologies in the Adult. Immunity 50, 1276–1288.e5 (2019). [PubMed: 30902637]
47. Sommereyns C, Paul S, Staeheli P & Michiels T IFN-lambda (IFN-λ) is expressed in a tissue-dependent fashion and primarily acts on epithelial cells in vivo. PLoS Pathog. 4, e1000017 (2008). [PubMed: 18369468]
48. Lin J-D et al. Distinct Roles of Type I and Type III Interferons in Intestinal Immunity to Homologous and Heterologous Rotavirus Infections. PLoS Pathog. 12, e1005600 (2016). [PubMed: 27128797]
49. Voss OH, Tian L, Murakami Y, Coligan JE & Krzewski K Emerging role of CD300 receptors in regulating myeloid cell efferocytosis. Mol. Cell. Oncol 2, e964625 [PubMed: 27308512]
50. Santiana M. et al. Vesicle-Cloaked Virus Clusters Are Optimal Units for Inter-organismal Viral Transmission. Cell Host Microbe 24, 208–220.e8 (2018). [PubMed: 30092198]
51. Henke-Gendo C. et al. New real-time PCR detects prolonged norovirus excretion in highly immunosuppressed patients and children. J. Clin. Microbiol 47, 2855–62 (2009). [PubMed: 19625473]
52. Nurminen K. et al. Prevalence of norovirus GII-4 antibodies in Finnish children. J. Med. Virol 83, 525–31 (2011). [PubMed: 21264875]
53. Newman KL & Leon JS Norovirus immunology: Of mice and mechanisms. Eur. J. Immunol 45, 2742–57 (2015). [PubMed: 26256101]
54. Simon AK, Hollander GA & McMichael A Evolution of the immune system in humans from infancy to old age. Proceedings. Biol. Sci 282, 20143085 (2015).
55. Mombaerts P. et al. RAG-1-deficient mice have no mature B and T lymphocytes. Cell 68, 869–77 (1992). [PubMed: 1547488]
56. Durbin JE, Hackenmiller R, Simon MC & Levy DE Targeted disruption of the mouse Stat1 gene results in compromised innate immunity to viral disease. Cell 84, 443–50 (1996). [PubMed: 8608598]
57. Muller U. et al. Functional role of type I and type II interferons in antiviral defense. Science 264, 1918–1921 (1994). [PubMed: 8009221]
58. Huang S. et al. Immune response in mice that lack the interferon-gamma receptor. Science 259, 1742–5 (1993). [PubMed: 8456301]
59. Wallner B. et al. Generation of mice with a conditional Stat1 null allele. Transgenic Res. 21, 217–24 (2012). [PubMed: 21553074]
60. Madison BB et al. Cis Elements of the Villin Gene Control Expression in Restricted Domains of the Vertical (Crypt) and Horizontal (Duodenum, Cecum) Axes of the Intestine. J. Biol. Chem 277, 33275–33283 (2002). [PubMed: 12065599]
61. Clausen BE, Burkhardt C, Reith W, Renkawitz R & Förster I Conditional gene targeting in macrophages and granulocytes using LysMcre mice. Transgenic Res. 8, 265–277 (1999). [PubMed: 10621974]
62. Ogilvy S. et al. Promoter elements of vav drive transgene expression in vivo throughout the hematopoietic compartment. Blood 94, 1855–63 (1999). [PubMed: 10477714]
63. Shimshek DR et al. Codon-improved Cre recombinase (iCre) expression in the mouse. Genesis 32, 19–26 (2002). [PubMed: 11835670]

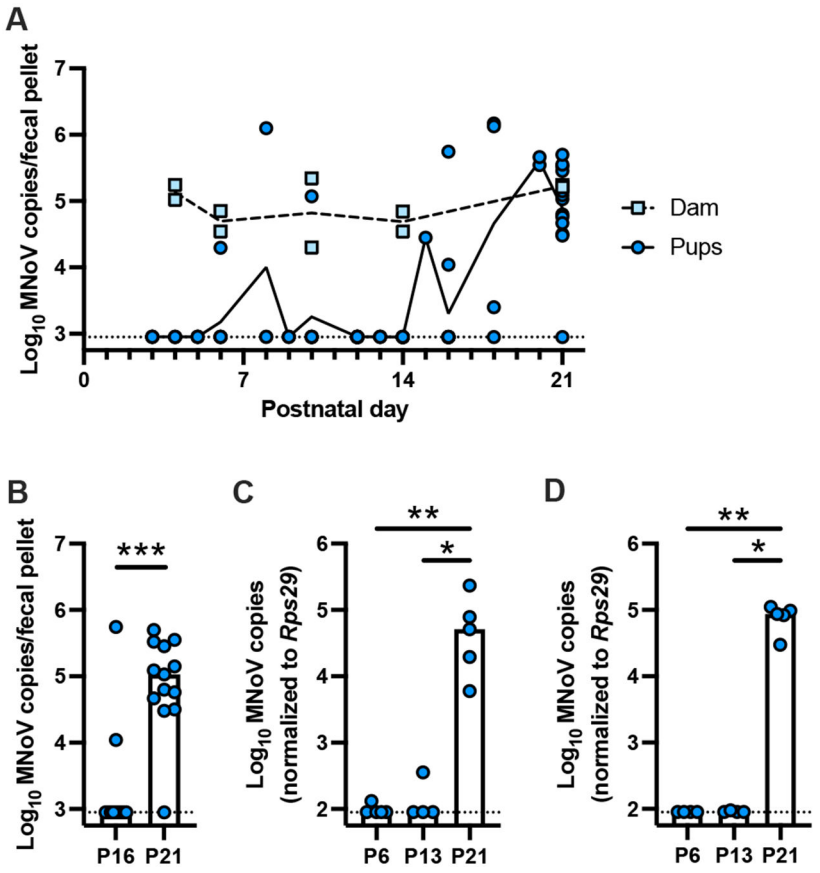

Figure 1: Natural transmission of persistent MNoV from infected dams occurs after postnatal day 16.

Pregnant C57BL/6 dams were orally inoculated with CR6 5-6 days prior to giving birth. **(A, B)** Fecal samples were collected from pups up to postnatal day (P)21, and MNoV genome copies detected by quantitative real-time PCR (qPCR). **(B)** is comparison of P16 and P21 fecal samples from **(A)**. Ileum **(C)** and colon **(D)** samples were collected and MNoV genome copies detected by qPCR. Analyzed by two-tailed Mann-Whitney test **(B)** or Kruskal-Wallis test with Dunn's multiple comparisons test (**C, D). (A)** n=22 pups from 3 litters. Given the challenge of obtaining stool from young mice, fecal samples were collected as possible; each data point indicates stool from a single mouse, with exact n for each timepoint in Source Data. **(B)** P16 (n=11) and P21 (n=13), ***p=0.009. **(C, D)** Samples from 2 litters were collected at P6 (n=5), P13 (n=4), and P21 (n=5). **(C)** *p=0.0204, **p=0.0073. **(D)** *p=0.0251, **p=0.0072. Dashed lines indicate limit of detection for assays.

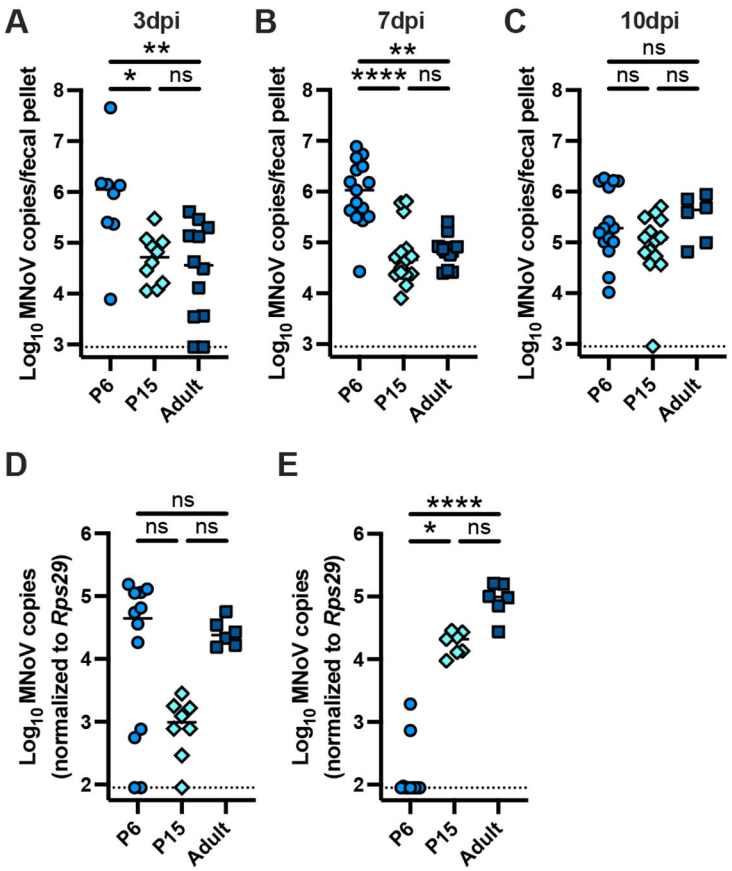

Figure 2: Inoculation of pups with persistent MNoV is associated with distinct localization.

C57BL/6 mice were orally inoculated with CR6 at P6, P15, or as adults (6-9 weeks old). **(A-C)** Fecal samples were collected at 3 days-post infection (dpi) **(A)** , 7dpi **(B)**, and 10 dpi **(C)**, and MNoV genome copies detected by qPCR. Ileum **(D)** and colon **(E)** samples were collected at 7dpi and MNoV genome copies detected by qPCR. Analyzed by one-way ANOVA with Holm-Šídák's multiple comparisons test **(A)** or Kruskal-Wallis test with Dunn's multiple comparisons test **(B-E)**. **(A)** P6 (n=8, 3 litters), P15 (n=10, 2 litters), adult (n=12, 2 independent experiments), *p=0.0160, **p=0.0033. **(B)** P6 (n=15, 4 litters), P15 (n=15, 3 litters), adult (n=12, 3 independent experiments), **p=0.0034, ****p<0.0001. **(C)** P6 (n=15, 5 litters), P15 (n=14, 3 litters), adult (n=6, 2 independent experiments). (**D, E**) P6 (n=12, 2 litters; sourced from Charles River), P15 (n=8, 2 litters), adult (n=6, 2 independent experiments). *p=0.0193, ****p<0.0001. Dashed lines indicate limit of detection for assays. ns = not significant (p>0.05).

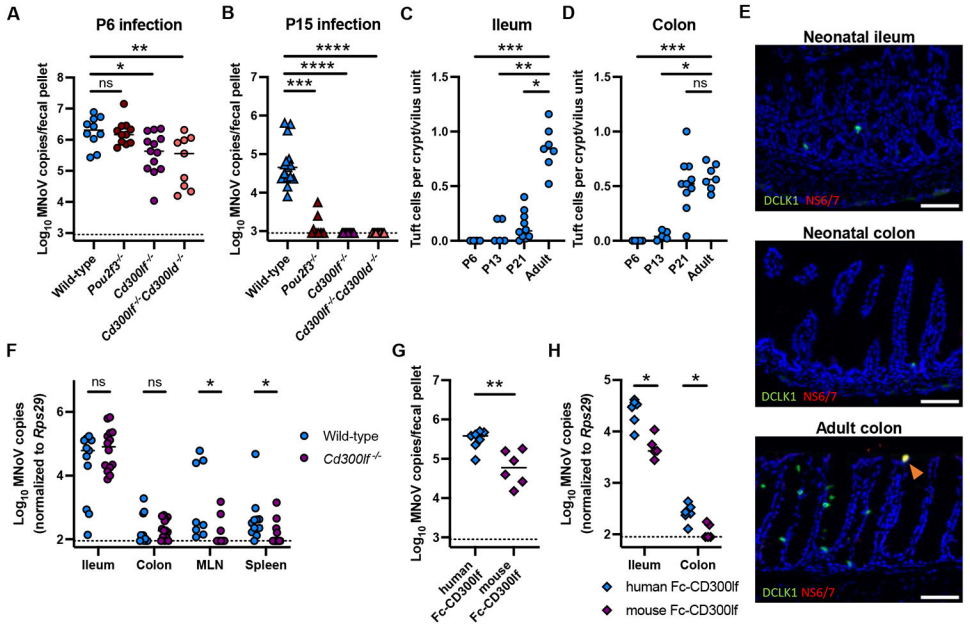

Figure 3: Tuft cells and CD300 family viral receptors have a limited role in neonatal viral RNA shedding.

(A, B) Mice were orally inoculated with CR6 at P6 **(A)** or P15 **(B)** and MNoV genome copies quantified from 7dpi stool samples by qPCR. **(C)** Tuft cells were quantified by immunofluorescent staining of DCLK1 in naïve wild-type mice. **(D)** Intestinal samples from mice orally inoculated with CR6 at P6 (neonatal) or as adults were collected at 7dpi and stained for DCLK1 and CR6 nonstructural protein NS6/7. Orange arrow indicates a CR6-infected tuft cell. Scale bars are 30μm. **(E)** Neonates were orally inoculated with CR6 at P6 and MNoV genome copies quantified from 7dpi samples by qPCR. **(F, G)** CR6 was preincubated with Fc-huCD300lf or Fc-msCD300lf prior to oral inoculation of C57BL/6 littermates at P6. Stool **(F)** and tissue **(G)** virus levels were quantified by qPCR at 7dpi. Analyzed by one-way ANOVA with Holm-Šídák multiple comparisons **(A)**, Kruskal-Wallis test with Dunn's multiple comparisons **(B, C)**, two-tailed Mann-Whitney test corrected with the Holm-Šídák method **(E, G)**, or two-tailed t-test **(F)**. **(A)** Wild-type (n=10, 3 litters), *Pou2f3*$^{-/-}$ (n=11, 2 litters), *Cd300lf*$^{-/-}$ (n=13, 4 litters), and *Cd300lf*$^{-/-}$*Cd300ld*$^{-/-}$ (n=9, 2 litters). *p=0.0235, **p=0.0046. **(B)** Wild-type (n=15, 3 litters), *Pou2f3*$^{-/-}$ (n=10, 3 litters), *Cd300lf*$^{-/-}$ (n=11, 2 litters), and *Cd300lf*$^{-/-}$*Cd300ld*$^{-/-}$ (n=11, 3 litters, ***p=0.0004 (wild-type vs. *Pou2f3*$^{-/-}$), ****p<0.0001 (wild-type vs. *Cd300lf*$^{-/-}$ and wild-type vs. *Cd300lf*$^{-/-}$*Cd300ld*$^{-/-}$). Wild-type 7dpi data overlaps with P6/P15 litters in Fig. 2B. **(C, D)** P6 (n=5), P13 (n=5), P21 (n=10), adult (n=7), each from 2 independent experiments. **(C)** Ileum: *p=0.0173, **p=0.0042, ***p=0.0003. Colon: *p=0.0257, ***p=0.0009. **(D)** Representative of four samples for neonatal ileum and colon. **(E)** Wild-type (n=12, 2 litters, sourced from Charles River) or *Cd300lf*$^{-/-}$ (n=14, 2 litters), *p=0.0185 (MLN, spleen). Wild-type ileum/colon data overlaps with Fig. 2D, E. **(F, G)** Fc-huCD300lf (n=7) and Fc-msCD300lf (n=6) from 2 litters, **p=0.0036. **(G)** *p=0.0172 (ileum), *p=0.0173 (colon). Dashed lines indicate limit of detection for assays. ns=not significant (p>0.05).

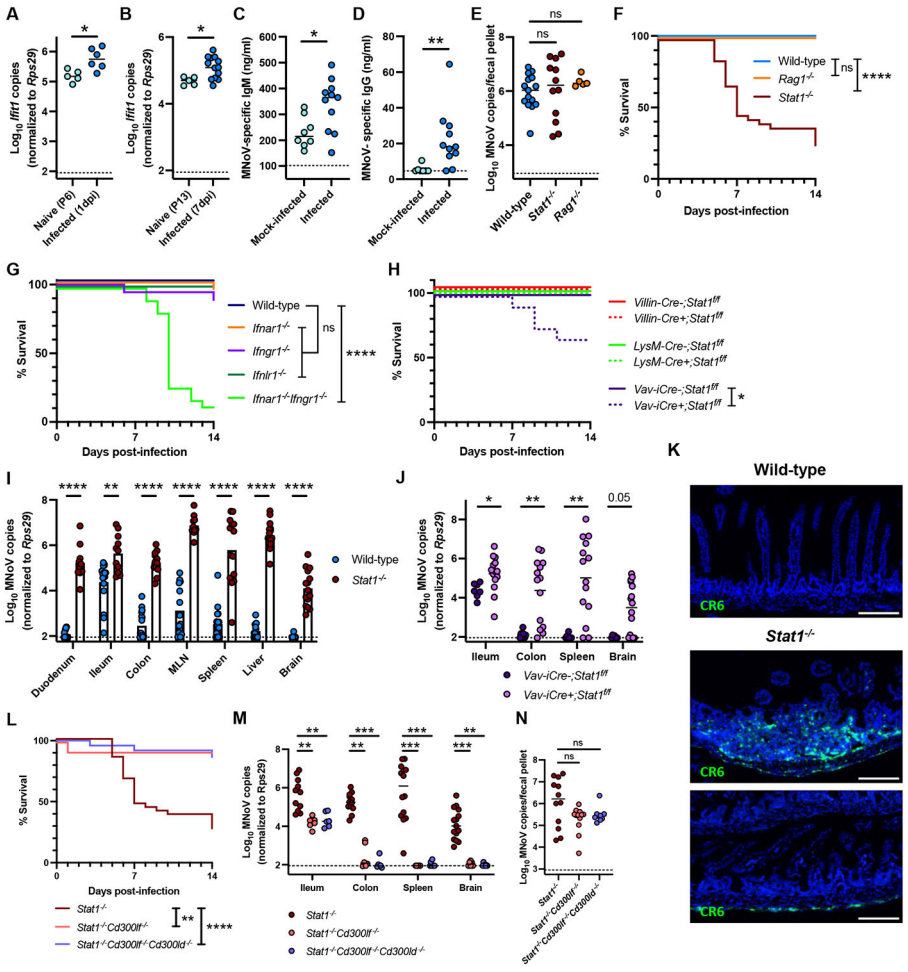

Figure 4: STAT1 signaling protects against lethality and extraintestinal CR6 spread in neonatal mice.

(A-D) Wild-type neonates were orally inoculated with CR6 at P6. *Ifit1* was quantified by qPCR from ilea collected at 1 **(A)** or 7 dpi **(B)** and compared to uninfected mice. Serum was collected at 14dpi and anti-MNoV IgM **(C)** and IgG **(D)** quantified by ELISA and compared to mock-infected mice. **(E-G)** Neonates were orally inoculated with CR6 at P6 and MNoV genome copies quantified from 7dpi stool samples by qPCR with wild-type stool as shown in Fig. 2B **(E).** Survival tracked through 14dpi with wild-type survival curve replicated in F and G **(F, G)**. **(H)** Littermates for each Cre line, born to Cre− dams bred to Cre+ sires, were orally inoculated with CR6 at P6 and survival tracked through 14dpi. **(I)** Neonates were orally inoculated with CR6 at P6 and tissues collected at 7dpi unless pups appeared ill and needed to be euthanized (5-6dpi). Tissue MNoV genome copies were quantified by qPCR **(J)** Littermates were orally inoculated with CR6 at P6 and tissue MNoV genome copies quantified at 6-7dpi. **(K)** Neonates were orally inoculated with CR6 at P6. Ilea were collected at 6-7dpi and stained for CR6 RNA using RNA-*in situ* hybridization. Scale bars are 50μm. **(L-N)** Neonates were orally inoculated with CR6 at P6 and survival tracked through 14dpi, with *Stat1*$^{-/-}$ survival curve replicated from F **(L)**. Tissues were collected at 5-7dpi **(M)** and stool collected at 7dpi **(N)** and MNoV genome copies quantified by qPCR, with *Stat1*$^{-/-}$ tissues and stool as in I and E

respectively. Analyzed by two-tailed t-test **(A, B, C)**, two-tailed Mann-Whitney test **(D)**, Welch's ANOVA (**E**), Gehan-Breslow-Wilcoxon test **(F, G, H, L),** two-tailed Mann-Whitney test corrected with the Holm-Šídák method **(I, J)**, Kruskal-Wallis test with Dunn's multiple comparisons test **(M, N)**. **(A)** Naïve (n=5, 1 litter), infected (n=6, 3 litters), **p=0.0071. **(B)** Naïve (n=5, 2 litters), infected (n=13, 4 litters), *p=0.0171. **(C, D)** Mock-infected (n=8, 2 litters), infected (n=11, 4 litters). **(C)** *p=0.0153. **(D)** **p=0.0016. **(E)** Wild-type (n=15, 4 litters), *Stat1*$^{-/-}$ (n=12, 5 litters), and *Rag1*$^{-/-}$ (n=5 , 1 litter). **(F)** Wild-type (n=21, 4 litters), *Stat1*$^{-/-}$ (n=34, 5 litters), and *Rag1*$^{-/-}$ (n=13, 2 litters), ****p<0.0001. **(G)** Wild-type (n=21, 4 litters), *Ifnar1*$^{-/-}$ (n=21, 4 litters), *Ifngr1*$^{-/-}$ (n=18, 3 litters), *Ifnlr1*$^{-/-}$ (n=24, 4 litters), and *Ifnar1*$^{-/-}$*Ifngr1*$^{-/-}$ (n=22, 4 litters), ****p<0.0001. **(H)** *Villin-Cre-;Stat1*$^{f/f}$ (n=9), *Villin-Cre+;Stat1*$^{f/f}$ (n=10), littermates from 3 litters; *Lysm-Cre-;Stat1*$^{f/f}$ (n=7), *Lysm-Cre+;Stat1*$^{f/f}$ (n=12), littermates from 3 litters; *Vav-iCre-;Stat1*$^{f/f}$ (n=14), *Vav-iCre+;Stat1*$^{f/f}$ (n=12), littermates from 4 litters. *p=0.0210. **(I)** Wild-type (n=18, 3 litters; brain collected from 6 neonates from 1 litter) and *Stat1*$^{-/-}$ (n=12, 3 litters). **p=0.0014 (ileum), ****p<0.0001 (duodenum, colon, MLN, spleen, brain). **(J)** *Vav-iCre+;Stat1*$^{f/f}$ (n=7), *Vav-iCre+;Stat1*$^{f/f}$ (n=15) littermates from 3 litters, *p=0.0248 (ileum), **p=0.0046 (colon), **p=0.0058 (spleen), p=0.0521 (brain). **(K)** Representative of n=5 wild-type ilea, n=6 *Stat1*$^{-/-}$ ilea. **(L)** *Stat1*$^{-/-}$ (n=34, 5 litters), *Stat1*$^{-/-}$*Cd300lf*$^{-/-}$ (n=7, 2 litters), and *Stat1*$^{-/-}$*Cd300lf*$^{-/-}$*Cd300ld*$^{-/-}$ (n=19, 3 litters), *p=0.0445, ***p=0.0003. **(M)** *Stat1*$^{-/-}$ (n=12, 3 litters), *Stat1*$^{-/-}$*Cd300lf*$^{-/-}$ (n=6, 2 litters), and *Stat1*$^{-/-}$*Cd300lf*$^{-/-}$*Cd300ld*$^{-/-}$ (n=6, 2 litters). **p=0.0019 (*Stat1*$^{-/-}$ vs· *Stat1*$^{-/-}$*Cd300lf*$^{-/-}$, ileum), **p=0.0082 (*Stat1*$^{-/-}$ vs. *Stat1*$^{-/-}$*Cd300lf*$^{-/-}$*Cd300ld*$^{-/-}$, ileum), **p=0.0069 (*Stat1*$^{-/-}$ vs. *Stat1*$^{-/-}$*Cd300lf*$^{-/-}$, colon), ***p=0.0002 (*Stat1*$^{-/-}$ vs. *Stat1*$^{-/-}$*Cd300lf*$^{-/-}$*Cd300ld*$^{-/-}$, colon), ***p=0.0002 (*Stat1*$^{-/-}$ vs. *Stat1*$^{-/-}$*Cd300lf*$^{-/-}$, spleen), ***p=0.0007 (*Stat1*$^{-/-}$ vs. *Stat1*$^{-/-}$*Cd300lf*$^{-/-}$*Cd300ld*$^{-/-}$, spleen), **p=0.0014 (*Stat1*$^{-/-}$ vs. *Stat1*$^{-/-}$*Cd300lf*$^{-/-}$, brain), ***p=0.0002 (*Stat1*$^{-/-}$ vs. *Stat1*$^{-/-}$*Cd300lf*$^{-/-}$*Cd300ld*$^{-/-}$, brain). **(N)** *Stat1*$^{-/-}$ (n=12, 5 litters), *Stat1*$^{-/-}$*Cd300lf*$^{-/-}$ (n=12, 2 litters), and *Stat1*$^{-/-}$*Cd300lf*$^{-/-}$*Cd300ld*$^{-/-}$ (n=9, 2 litters). Dashed lines indicate limit of detection for assays. ns, not significant (p>0.05).

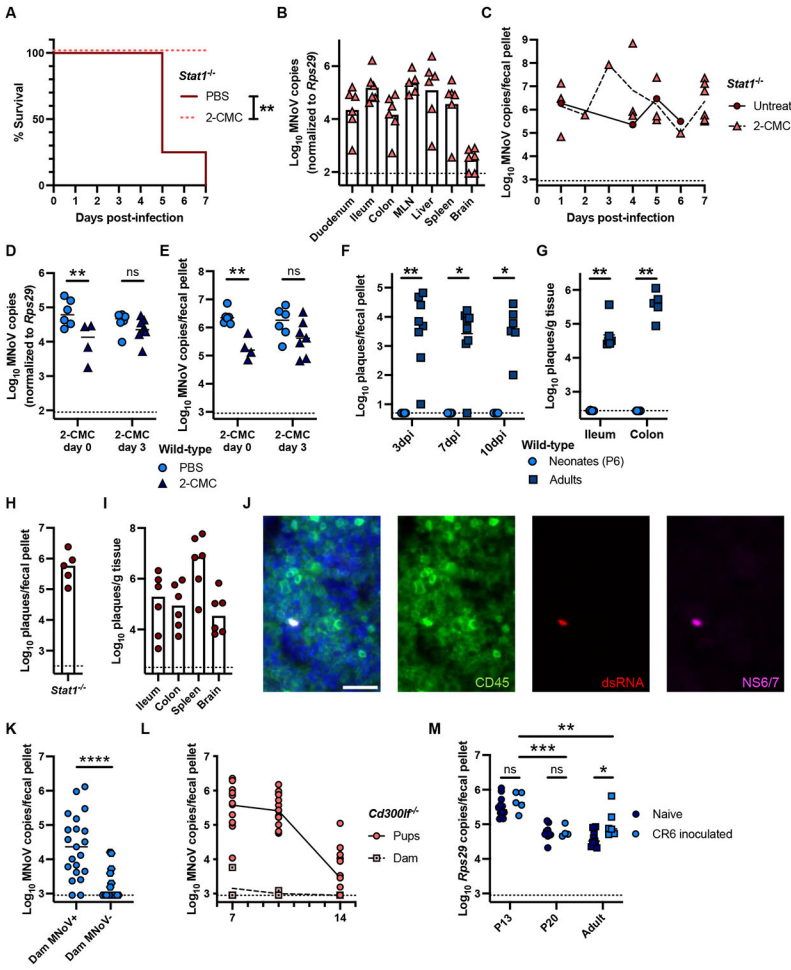

Figure 5: Persistent MNoV replicates in neonates in the absence of STAT1 signaling.

(A-C) *Stat1*$^{-/-}$ pups were orally inoculated with CR6 at P6. 100mg/kg 2-CMC or PBS was injected subcutaneously daily to littermates beginning at 3dpi and survival tracked through 7dpi. Tissues were collected at 7dpi (**B**) and stool collected at 1-7dpi (**C**) and MNoV genome copies quantified by qPCR. **(D, E)** Wild-type pups were orally inoculated with CR6 at P6. 100mg/kg 2-CMC or PBS were injected subcutaneously daily to littermates beginning at 0dpi or 3dpi. Ilea (**D**) and stool (**E**) were collected at 7dpi and MNoV genome copies quantified by qPCR. **(F, G)** Wild-type neonates (P6) and adults (6-9 weeks old) were orally inoculated with CR6. Infectious virus from 3-10dpi stool **(F)** and 7dpi tissues **(G)** was quantified by plaque assay on BV2 cells. **(H, I)** *Stat1*$^{-/-}$ neonates were orally inoculated with CR6 at P6. Infectious virus from stool **(H)** and tissues (**I**) collected at 5-6 dpi was quantified by plaque assay on BV2 cells. (**J**) *Stat1*$^{-/-}$ pups were orally inoculated with CR6 at P6. Spleen samples were collected at 5dpi and stained for CD45, dsRNA, and NS6/7. Scale bar is 30um. (**K**) Wild-type neonates were orally inoculated with CR6 at P6 and fecal pellets collected from dam and pups at 14dpi. MNoV genome copies were quantified by qPCR and MNoV+ dams defined as those with MNoV genome copies above the limit of detection. (**L**) *Cd300lf*$^{-/-}$ neonates were inoculated with CR6 at P6 and fecal pellets collected from dam and pups at 7, 10, and 14dpi and MNoV genome copies

quantified by qPCR, with 7dpi pup stool replicated from Fig. 3A. (**M**) *Rps29* expression was assessed by qPCR in stool samples from wild-type naïve and CR6-inoculated neonates (inoculated at P6, collected at P13, P20) or adult mice (naïve vs. 14dpi). Analyzed by Gehan-Breslow-Wilcoxon test **(A)**, two-way ANOVA with Šídák's multiple comparisons test **(D, E)**, two-tailed Mann-Whitney test corrected with the Holm-Šídák method **(F, G)**, two-tailed Mann-Whitney test **(K)**, two-way ANOVA with Tukey's multiple comparisons **(M)**. **(A-C)** 2-CMC (n=6), PBS (n=4), from two litters. **(A)** **p=0.0023. **(D, E)** Day 0 PBS (n=6), 2-CMC (n=4), from two litters; Day 3 PBS (n=6), 2-CMC (n=8), from two litters. **(D)** **p=0.0055. (**E**) **p=0.0051. **(F)** P6 (n=5, 3dpi; n=7, 7dpi; n=4, 10dpi; from two litters) and adult (n=8, 3dpi; n=9, 7dpi; n=6, 10dpi; from two experiments). **p=0.0047 (3dpi), *p=0.0113 (7dpi, 10dpi). **(G)** P6 (n=6; from two litters) and adult (n=6; from two experiments), **p=0.0043 (ileum and colon). **(H, I)** n=6, from 2 litters. **(J)** Representative of three independent samples. **(K)** MNoV+ pups (n=21, from 5 litters), MNoV− pups (n=20, from 5 litters), ****p<0.0001. **(L)** n=20, from 3 litters. **(M)** Naïve pups (n=12, 2 litters), CR6 pups (n=6, 3 litters), naïve adults (n=11, 2 experiments), CR6-inoculated adults (n=6, 1 experiment), *p=0.0285, **p=0.0073, ***p=0.0004.
Dashed lines indicate limit of detection for assays. ns, not significant (p>0.05).

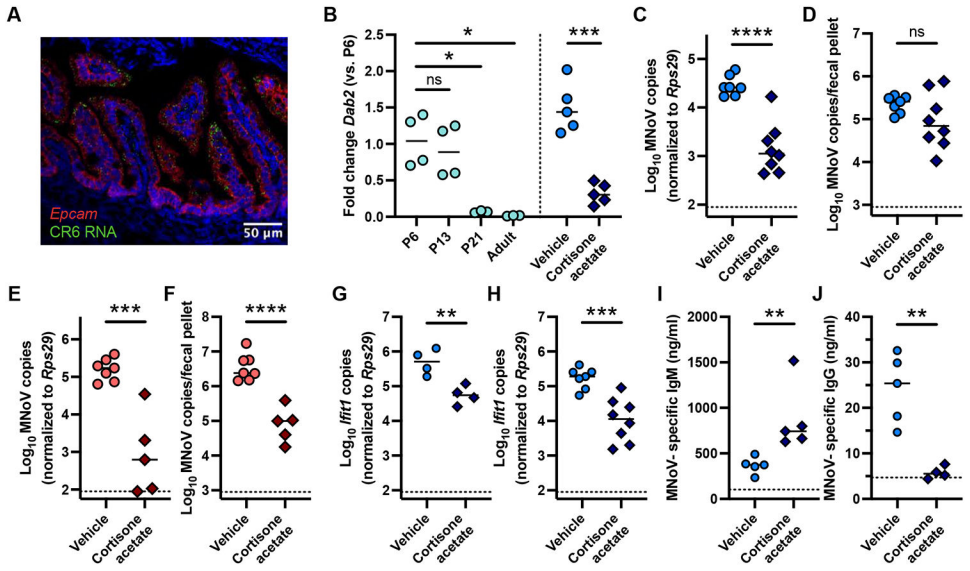

Figure 6: Non-specific uptake leads to the accumulation of persistent MNoV RNA in neonatal small intestines.

(A) Wild-type neonates were orally inoculated with CR6 at P6 and ilea collected at 8hpi and stained for CR6 and *Epcam* RNA using RNA-*in situ* hybridization. (**B**) Ileal samples were collected from naïve mice at P6, P13, P21, and as adults (left) or at 7dpi (P13) from littermates inoculated with CR6 and treated subcutaneously with 0.5mg/g cortisone acetate or vehicle at P6 (right). *Dab2* expression was quantified by qPCR. (**C, D**) Wild-type littermates were orally inoculated with CR6 and injected subcutaneously with 0.5mg/g cortisone acetate or vehicle at P6. 7dpi ilea **(C)** and stool **(D)** MNoV genome copies were quantified by qPCR. (**E, F**) *Cd300lf*$^{-/-}$ littermates were inoculated with CR6 and treated subcutaneously with 0.5mg/g cortisone acetate or vehicle at P6. 7dpi ilea **(E)** and stool **(F)** MNoV genome copies were quantified by qPCR. (**G-J**) Wild-type neonates were orally inoculated with CR6 and treated subcutaneously with 0.5mg/g cortisone acetate or vehicle at P6. *Ifit1* expression at 1dpi (**G**) and 7dpi (**H**) was quantified by qPCR. Serum was collected at 14dpi and anti-MNoV IgM (**I**) and IgG (**J**) were quantified by ELISA, with vehicle data overlapping with Fig. 4A-D. Analyzed by Welch's ANOVA with Dunnett's multiple comparisons test (**B,** time course), two-tailed t-test (**B,** vehicle vs cortisone acetate, **E**, **F**, **G**, **H**, **J**), Welch's two-tailed t test **(C, D)**, and two-tailed Mann-Whitney test **(I). (A)** Representative sample; remaining replicates shown in Extended Data Fig. 8. **(B)** P6 (n=4,1. litter), P13 (n=4, 2 litters), P21 (n=3, 2 litters), adult (n=3, 1 experiment), 7dpi cortisone acetate (n=5, 2 litters), 7dpi vehicle (n=5, 2 litters). *p=0.0283 (P6 vs. P21), *p=0.0243 (P6 vs. adult), ***p=0.0001 (vehicle vs. cortisone acetate). **(C, D)** Cortisone acetate (n=8) or vehicle (n=7), from 3 litters. **(C)** ****p<0.0001. **(E, F)** Cortisone acetate (n=5) or vehicle (n=7), from 2 litters. **(E)** ***p=0.0003. **(F)** ****p<0.0001. (**G**) 2 independent litters (4 pups/group), **p=0.0061. (**H**) 3 independent litters (7-8 pups/group), analyzed by two-tailed t test, ***p=0.0004. **(I, J)** 2 independent litters (5 pups/group). **(I)** **p=0.0079. **(J)** **p=0.0022. Dashed lines indicate limit of detection for assays. ns, not significant (p>0.05).